

RESEARCH

Open Access

Multi-tier dynamic sampling weak RF signal estimation theory



Brett Smith¹ and Mary Lanzerotti^{1*}

*Correspondence:
marylanzerotti@vt.edu

¹ Bradley Department of Electrical and Computer Engineering, Virginia Polytechnic Institute and State University, Blacksburg, VA, USA

Abstract

This paper presents a theoretical analysis in discrete time for a multi-tier weak radiofrequency (RF) signal estimation process with N simultaneous signals. Discrete time dynamic sampling is introduced and is shown to provide the capability to extract signal parameter values with increased accuracy compared with accuracy of estimates obtained in prior work. This paper advances phase measurement approaches by proposing discrete time dynamic sampling which our paper shows offers the desirable capability for more accurate weak signal parameter estimates. For $N = 2$ simultaneous signals with a strong signal at 850 MHz and a weak signal at 855 MHz, the results show that dynamically sampling the instantaneous frequency at 24 times the Nyquist rate provides weak signal frequency estimates that are within 1.7×10^{-5} of the actual weak signal frequency and weak signal amplitude estimates that are within 428 PPM of the actual weak signal amplitude. Results are also presented for situations with $N = 2$ simultaneous 5G signals. In one case, the strong signal is 3950 MHz, and the weak signal is 3955 MHz; in the other case the strong case is 5950 MHz, and the weak signal is 5955 MHz. The results for these cases show that estimates obtained with dynamic sampling are more accurate than estimates provided using a single sample rate of 65 MSPS. This work has promising applications for weak signal parameters estimation using instantaneous frequency measurements.

Keywords: Electronic warfare (EW), Radiofrequency (RF), Signal processing, Dynamic processing, Phase calculation approaches, 5G, Multirate digital signal processing

1 Introduction

The problem of determining accurate weak signal parameter estimates is of interest in instantaneous frequency measurements in electronics and photonics. In electronics, research has focused in the areas of electronic warfare (EW) systems, instantaneous frequency receivers, complex communication, wireless communication, radar signal estimation and detection [1, 2], anti-stealth defense, miniaturized instrumentation and control systems for air and space applications, electronic support measures (ESM) [3], and electronic intelligence [4].

Instantaneous frequency receivers were designed in the 1950s in Great Britain by Robinson and colleagues [5–10]. Prior work explored alternative approaches to multiple signal detection [11–15], cognitive radio, and software-defined radio. In 2017, Digne et al.

discuss their aim to extract features from instantaneous frequency measurements in a naval electronic warfare context [2]. In 2019, Raviteja et al. [16] proposed orthogonal time frequency space (OTFS) modulation as a way to “tackle destructive Doppler effects in wireless communications” [16] for radar and communications and related applications. The aim of OTFS-based filter algorithms provide “improved radar capability, such as longer range, faster tracking rate, as well as larger Doppler frequency estimation” [16]. The use of synthetic aperture passive positioning methods are proposed for determining the frequency of a frequency-hopping (FH) signal for passive localization of radio emitters [17] and radar signal estimation in low signal-to-noise environments [18]. Dong et al. discuss signal parameters of signals in satellite data (1.7 GHz carrier frequency and 5 kHz channel spacing) [17]. Alphonse et al. estimate signal parameters for frequency-modulated radar signals [18].

In photonics, research has focused on methods for instantaneous frequency measurements that have potential for use in instantaneous frequency receivers [19–29]. Liang et al. designed, built, and tested an instantaneous measurement system with 4 GHz center frequency and 500 MHz bandwidth using high-temperature superconducting (HTS) devices made of Yttrium Barium Copper Oxide (YBCO) [19]. Khalil et al. built an on-chip circuit in 0.25 μm CMOS technology that measures the on-chip phase-noise spectrum and clock jitter [20]. Lam et al. discuss an instantaneous frequency measurement receiver with a photonic time stretch analog-to-digital converter (ADC) with the capability for “ultra-fast sweeping across enormous bandwidths to perform measurements on transient signals” [21]. The receiver built by Lam et al. was capable of resolving two signals (tones) with a 14 dB strong signal with 8 GHz frequency and a 5 dB weaker signal with 9 GHz frequency. Goavec et al. describe an instantaneous frequency measurement system designed and built in 130 μm CMOS technology to measure a pulse in an ultra-wide band frequency band (3.1–4.9 GHz) [22]. Wang and Pan [23] and Pan and Yao [24] performed photonics-based measurements of microwave signal parameters including electric field measurements and phase noise measurements. They note that “microwave photonic techniques can be employed to extend the bandwidth of IFM receivers to tens or even hundreds of GHz and also offer the advantage of immunity to EMI [electromagnetic interference]” [24]. They also measured the Doppler frequency shift of microwave signals. Tang et al. [27] and Zhou et al. [28] performed photonics-based instantaneous frequency measurements and resolve two signals with frequency 7GHz and 7.02GHz having frequency separation of 20 MHz. Also in 2023, Bai et al. performed ultra-wideband instantaneous frequency measurements in real time [29] with 660 MHz resolution and ± 380 MHz measurement error. The system developed by Bai et al. “can perform single- and multiple-frequency measurements over a range of 3–20 GHz” [29].

2 Reconfigurable multi-rate digital signal processing

Multi-rate digital signal processing (MR DSP) applications are accomplished with decimation to reduce the sample rate, interpolation to increase the sample rate, and a combination of decimation and interpolation. Baldini et al. [30] describe considerations for circuits and systems that need to be taken into account in designing reconfigurable receivers. LeRoy et al. [31] describe circuits for use in reconfigurable multi-rate

digital signal processing applications. They designed, built, and tested custom circuits comprised of SiGe heterojunction bipolar transistors (HBT) to enable ultrafast reconfigurability for applications including software-defined radio, multi-rate digital signal processing, and optical communications. SiGe HBT technology offers high performance (cutoff frequency $f_T = 300$ GHz) and integration with CMOS circuits on silicon wafers. SiGe HBT transistors have been used to build high-speed ADCs, field programmable gate arrays (FPGAs), multi-rate adaptive filters, and voltage-controlled oscillators (VCOs). ADCs sample an analog signal at a specified sample rate and produce a digital signal. Quantifying the quantization error in an N -bit ADC is important because obtaining accurate weak signal parameter estimates needs to take into account the quantization error introduced by an ADC [32].

3 Review of our prior work on phase calculation approaches for a weak signal estimation process

The aim of our research is to design an electronic warfare (EW) receiver with capability to receive $N = 4$ simultaneous signals. This section reviews our prior work in which we presented theoretical analysis of a multi-tier weak radiofrequency (RF) signal estimation process for N simultaneous signals [33–39]. This work developed from the work of James Tsui [40]. In these processes, one signal is strong, and the rest of the signals ($N - 1$) are weak. In this work, as in prior work, the term *weak* refers to a signal with much lower amplitude compared to the amplitude of the strong signal. The term *strong* refers to the signal that has the maximum amplitude. The amplitude of each weak signal is normalized to the amplitude of the strong signal, and so the amplitude of the strong signal is set to unity ($R_1 = 1$). The amplitudes of the weak signals are less than unity. Our work generalizes James Tsui's prior phase measurement approaches for estimating weak signal parameters in the presence of a strong interfering signal [33–40]. We extract weak signal parameters in real time using zero crossings that occur in the instantaneous frequency. We demonstrated theoretically that our approach is capable of estimating the weak signal parameters of a weak signal in the presence of a strong signal (that is, two simultaneous signals). Our prior results considered $N = 2$ simultaneous signals with a *strong* signal with frequency 850 MHz and a *weak* signal with frequency 855 MHz. The sample period was $\frac{1}{2\pi}$ μ s. The results showed that the weak signal frequency estimates are within 0.5 PPM of the weak signal, and weak signal amplitude estimates are within 0.12 % of the weak signal amplitude [37].

Our prior work also took into account additive white Gaussian noise (AWGN) [38, 39]. We extracted weak signal parameters in real time using zero crossing clusters in the instantaneous frequency since the presence of noise introduces a cluster of zero crossings. Results of this work employing the analysis of zero crossing clusters showed that our weak signal estimation process provided weak signal frequency estimates to within 120 PPM of the weak signal frequency for a strong signal frequency of 850 MHz, a weak signal frequency of 855 MHz, a signal-to-interference ratio of 10^{-4} , and the weak signal-to-noise ratio is 20 dB, 30 dB, and 40 dB [39].

We now briefly review a derivation of the instantaneous frequency for the general situation in continuous time for N simultaneous signals, where one signal is *strong*, $N - 1$ signals are *weak*, and each signal takes on a constant amplitude and constant frequency for

a specified amount of time [33–40]. This time interval is referred to as a *tier*. For example, in a three-tier process, the weak signal parameters (weak signal frequency and weak signal amplitude) may take on different constant values in each of the three tiers. As discussed in [40], the strong signal $s_1(t)$ is

$$s_1(t) = e^{-j2\pi f_0 t} e^{j2\pi f_1 t}, \quad (1)$$

where f_0 represents the local oscillator frequency, and f_1 represents the strong signal frequency. There are $2 \leq k \leq N$ weak signals, and each weak signal $s_k(t)$ is,

$$s_k(t) = R_k e^{-j2\pi f_0 t} e^{j2\pi f_k t} e^{j\phi_k(t)}, \quad (2)$$

where we use the same notation as in prior work: f_k represents the k th weak signal frequency, where $f_k \neq f_1$; $\phi_k(t)$ is the phase difference between the k th signal and the local oscillator (the reference signal); $R_k \geq 0$ represents the amplitude of the k th signal. The combined signal $s_N(t)$ is the sum of all of the individual signals,

$$s_N(t) = \sum_{k=1}^N s_k(t), \quad (3)$$

$$= e^{-j2\pi f_0 t} e^{j2\pi f_1 t} \left(1 + \sum_{k=2}^N R_k e^{j2\pi \Delta f_{k1} t} e^{j\phi_k(t)} \right), \quad (4)$$

where $\Delta f_{k1} = f_k - f_1$.

The instantaneous frequency $f_N(t)$ for N simultaneous signals [33–40] is obtained from the real component $p_N(t)$ and imaginary component $q_N(t)$ of the combined signal $s_N(t)$ as well as the first derivative of the real component $\frac{dp_N(t)}{dt}$ and the first derivative of the imaginary component $\frac{dq_N(t)}{dt}$,

$$f_N(t) = \frac{1}{2\pi} \frac{d\theta_n(t)}{dt}, \quad (5)$$

$$= f_1 + \frac{1}{2\pi} \left[\frac{p_N(t) \frac{dq_N(t)}{dt} - q_N(t) \frac{dp_N(t)}{dt}}{p_N^2(t) + q_N^2(t)} \right], \quad (6)$$

where the phase $\theta_N(t)$ of the combined signal is

$$\theta_N(t) = 2\pi f_1 t + \tan^{-1} \left[\frac{q_N(t)}{p_N(t)} \right], \quad (7)$$

and

$$p_N(t) = 1 + \sum_{k=2}^N R_k \cos [2\pi (\Delta f_{k1} t + \phi_k(t))], \quad (8)$$

$$q_N(t) = \sum_{k=2}^N R_k \sin [2\pi (\Delta f_{k1} t + \phi_k(t))], \quad (9)$$

$$\frac{dp_N(t)}{dt} = - \sum_{k=2}^N R_k \left(2\pi \Delta f_{k1} + \frac{d\phi_k(t)}{dt} \right), \quad (10)$$

$$\times \{ \sin [2\pi (\Delta f_{k1} t + \phi_k(t))] \}, \quad (11)$$

$$\frac{dq_N(t)}{dt} = \sum_{k=2}^N R_k \left(2\pi \Delta f_{k1} + \frac{d\phi_k(t)}{dt} \right), \quad (12)$$

$$\times \{ \cos [2\pi (\Delta f_{k1} t + \phi_k(t))] \}, \quad (13)$$

respectively.

In prior work, we considered the case in which there were an arbitrary number of simultaneous signals, where one of the signals is *strong*, and $N - 1$ signals are *weak* [33–39]. One drawback of the previous analysis is that the approach used a continuous time formulation and assumed a single sample rate. A consequence of the assumption of a single sample rate is that the relative error in the weak signal frequency estimates takes on different values. Another consequence of the assumption of a single sample rate is that the error provided by the weak signal estimation process depends on where the sampled values are taken at each point in time, because the sample estimates of the instantaneous frequency are in general time varying since the weak signal frequency is unknown, can take on different values in each time interval (tier), and in general the weak signal frequency itself can be time varying.

This paper provides accurate weak signal parameter estimates through phase calculation approaches that determine a different sample rate in each tier in real time. The values of the sample rate are quantified as a multiple of the Nyquist rate of the instantaneous frequency.

This paper provides closed form solutions for a multi-tier weak signal estimation process in *discrete time* (DT). The approach starts from first principles using discrete time analysis and makes no approximations based on the weak signal magnitudes. A significant benefit of our approach is that this general treatment can be applied to many discrete-time signal processing problems and provide accurate weak-signal estimates using multi-rate digital signal processing.

This paper derives the equations for weak signal parameter estimates in discrete time in a multi-tier signal detection process for N simultaneous signals. As in prior work [33–39], we consider N simultaneous signals with constant amplitude and constant frequency in a series of tiers.

The contributions of this paper are:

- *Discrete time* analytical expressions for the instantaneous frequency and combined signal amplitude of N simultaneous signals, where each weak signal takes on a constant amplitude and constant frequency;
- *Discrete time* theoretical analysis including weak signal parameter estimates of the situation in which the sample rate is a multiple of the frequency of the instantaneous frequency in each tier of a multi-tier process;
- Accurate weak signal frequency estimates obtained with dynamic sampling in a discrete time multi-tier weak signal estimation process for $N = 2$ simultaneous RF and 5G signals;

The rest of the paper is as follows. Section 4 presents *discrete time* dynamic sampling phase calculation approaches for weak signal estimation. Section 5 discusses weak RF signal estimation process with dynamic sampling for $N = 2$ simultaneous signals. Section 6 discusses weak 5G simultaneous signals with a strong signal at 3950 MHz and a weak signal at 3955 MHz, and Section 7 presents a discussion and conclusions. The Appendix discusses weak 5G simultaneous signals with a strong signal at 5950 MHz and a weak signal at 5955 MHz.

4 Discrete time dynamic sampling phase calculation approaches for weak signal parameter estimation

We revisit the situation [33–39] in which the amplitude and frequency of each weak signal take on a different constant value in each tier l . In this paper, we now map from continuous time t (CT) in prior work to discrete time n (DT) in this paper for a multi-tier system with tier l by setting

$$t = nT_{s,l} \quad (14)$$

where sample n is a positive integer ($n \geq 0$), and $T_{s,l}$ is the sample period in tier l . For the k th weak signal, the difference $\Delta f_{k1,l}$ between the strong signal frequency f_1 and the weak signal frequency f_{k_l} in tier l is $\Delta f_{k1,l} = f_{k_l} - f_1$.

We represent the strong signal $s_1(n)$ and each weak signal $s_k(n)$ as

$$s_1(n) = e^{-j2\pi f_0 n T_{s,l}} e^{j2\pi f_1 n T_{s,l}}, \quad (15)$$

$$s_k(n) = R_{k_l} e^{-j2\pi f_0 n T_{s,l}} e^{j2\pi f_k n T_{s,l}} e^{j\phi_k(n T_{s,l})}, \quad (16)$$

where f_0 and f_1 represent the frequencies of the local oscillator and strong signal, respectively; $t = nT_{s,l}$ (Eq. 14); $2 \leq k \leq N$ is the index of the k th weak signal in tier l ; $f_k \neq f_1$ is the frequency of the k th weak signal; $\phi_k(n T_{s,l})$ is the phase difference between the phase of the k th signal and the phase of the local oscillator (the reference signal); the term $R_{k_l} \geq 0$ is the constant amplitude of the k th signal in tier l .

The combined signal, $s_N(n)$, is the sum of the contributions of the individual signals in each tier l with Eq. 14 as

$$s_N(n) = \sum_{k_l=1}^N s_{k_l}(n T_{s,l}), \quad (17)$$

$$= e^{-j2\pi f_0 n T_{s,l}} e^{j2\pi f_1 n T_{s,l}} \left(1 + \sum_{k_l=2}^N R_{k_l} e^{j2\pi \Delta f_{k_l} n T_{s,l}} e^{j\phi_{k_l}(n T_{s,l})} \right). \quad (18)$$

The combined signal $s_N(n)$ and the combined signal amplitude $E_N(n)$ are

$$s_N(n) = e^{-j2\pi f_0 n T_{s,l}} E_N(n T_{s,l}) e^{j\theta_N(n T_{s,l})}, \quad (19)$$

$$E_N(n) = \sqrt{[p_N(n)]^2 + [q_N(n)]^2}, \quad (20)$$

where $p_N(n)$ and $q_N(n)$ are the real and imaginary parts, respectively, of the combined signal,

$$p_N(n) = 1 + \sum_{k_l=2}^N R_{k_l} \cos(2\pi \Delta f_{k_l} n T_{s,l} + \phi_{k_l}(n T_{s,l})), \quad (21)$$

$$q_N(n) = \sum_{k_l=2}^N R_{k_l} \sin(2\pi \Delta f_{k_l} n T_{s,l} + \phi_{k_l}(n T_{s,l})), \quad (22)$$

The instantaneous phase $\theta_N(n)$ and instantaneous frequency $f_N(n)$ are

$$\theta_N(n) = 2\pi f_1 t + \tan^{-1} \left[\frac{q_N(n T_{s,l})}{p_N(n T_{s,l})} \right], \quad (23)$$

$$f_N(n) = f_1 + \frac{1}{2\pi} \frac{p_N(n T_{s,l}) \frac{dq_N(t)}{dt} \Big|_{t=n T_{s,l}} - q_N(n T_{s,l}) \frac{dp_N(t)}{dt} \Big|_{t=n T_{s,l}}}{p_N^2(n T_{s,l}) + q_N^2(n T_{s,l})}, \quad (24)$$

where $\phi_{k_l}(n) = 0$.

For two simultaneous signals, $N = 2$, the instantaneous frequency $f_{N=2,l}(n)$ in tier l is

$$f_{N=2,l}(n) = f_1 + \frac{R_{2,l} \Delta f_{21,l} \{\cos[2\pi(\Delta f_{21,l}) n T_{s,l}] + R_{2,l}\}}{1 + 2R_{2,l} \cos[2\pi(\Delta f_{21,l}) n T_{s,l}] + R_{2,l}^2}, \quad (25)$$

where $f_{2,l}$ and $R_{2,l}$ are the weak signal frequency and weak signal amplitude, respectively, in tier l , and where $\Delta f_{21,l} = f_{2,l} - f_1$.

The period of the instantaneous frequency $T_{N=2,l}$ in tier l is

$$T_{N=2,l} = \frac{1}{f_{2,l} - f_1}, \quad (26)$$

$$= \frac{1}{\Delta f_{21,l}}. \quad (27)$$

Weak signal parameter estimates are extracted from values of the z th and $(z + 2)$ th zero crossings in the instantaneous frequency in each tier l .

The z th and $(z + 2)$ th pair are chosen so that the zero crossings are both rising zero crossings (that is, the instantaneous frequency is increasing at both zero crossing) or both falling zero crossings (that is, the instantaneous frequency is decreasing at both zero crossings). The terms $\tilde{f}_{2,z,l}$ and $\tilde{R}_{2,z,l}$ refer to the weak signal frequency estimate and weak signal amplitude estimate, respectively, in tier l .

The Nyquist rate $f_{N,N=2,l}$, sample rate $f_{s,l}$, and sample period $T_{s,l}$ in tier l are

$$f_{N,N=2,l} = 2(f_{2,l} - f_1), \tag{28}$$

$$f_{s,l} = 2N_M(f_{2,l} - f_1), \tag{29}$$

$$T_{s,l} = \frac{1}{2N_M(f_{2,l} - f_1)}. \tag{30}$$

where N_M represents a multiple of the Nyquist rate $f_{N,N=2,l}$.

Figure 1 shows the instantaneous frequency $f_{N=2}(n)$ sampled with $N_M = 4.1$ showing odd zero crossings (for example, $z = 1$ and $z = 3$). The figure shows samples $n_{z=1,1,l=1}$, $n_{z=1,2,l=1}$ just before and just after the first zero crossing, first zero crossing sample estimate $\tilde{n}_{N=2,z=1,l=1}$, samples $n_{z=3,1,l=1}$, $n_{z=3,2,l=1}$ just before and just after the third zero crossing, and third zero crossing sample estimate $\tilde{n}_{N=2,z=3,l=1}$. The red “x” indicate the estimated zero crossings obtained by linear interpolation between the sample values just before and just after the zero crossings.

Figure 2 shows the instantaneous frequency $f_{N=2}(n)$ sampled with $N_M = 4.1$ showing even zero crossings (for example, $z = 2$ and $z = 4$) (Tables 1, 2).

Figure 3 shows the relative error in the weak signal frequency $\frac{\tilde{f}_{2,z,l} - f_{2,z,l}}{f_{2,z,l}}$ in tier l as a function of N_M for estimates obtained with first (downward) zero crossing ($z_{l=1} = 1$) and third (downward) zero crossing ($z_{l=1} = 3$) in tier $l = 1$; (a) N_M from 3.5 to 26.0; (b) N_M from 22.7 to 25.3. The red dots are values of relative error in weak signal frequency estimates obtained using linear interpolation to estimate first and third downward zero crossings and show good agreement with the predicted relative error.

In the limit in which the weak signal is much weaker than the strong signal, $R_{2,l} \ll R_1$, the instantaneous frequency $f_{N=2,l}(n)$ in tier l is

Table 1 Relative error in weak signal frequency estimates $\frac{\tilde{f}_{2,z,l} - f_{2,z,l}}{f_{2,z,l}}$ for ten values of N_M (see Fig. 3)

N_M	$\frac{\tilde{f}_{2,z,l} - f_{2,z,l}}{f_{2,z,l}}$
4.1	-1.698337042
4.5	0.008771943
6.5	-0.017543807
8.3	1.66129052
10	-0.008771917
10.3	0.880249437
15.3	-0.225137531
20.3	0.09649282
23.0	-0.008771917
23.5	-0.002923975

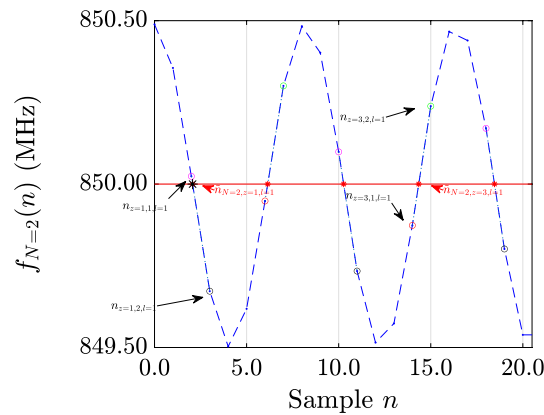


Fig. 1 Instantaneous frequency $f_{N=2}$ sampled with $N_M = 4.1$ showing odd zero crossings ($z = 1$ and $z = 3$): samples just before and just after the first zero crossing, $n_{z=1,1,l=1}, n_{z=1,2,l=1}$, first zero crossing sample estimate $\tilde{n}_{N=2,z=1,l=1}$, samples just before and just after the third zero crossing, $n_{z=3,1,l=1}, n_{z=3,2,l=1}$, third zero crossing sample estimate $\tilde{n}_{N=2,z=3,l=1}$. The red “x” indicate the estimated zero crossings obtained by linear interpolation between the sample times just before and just after the zero crossings

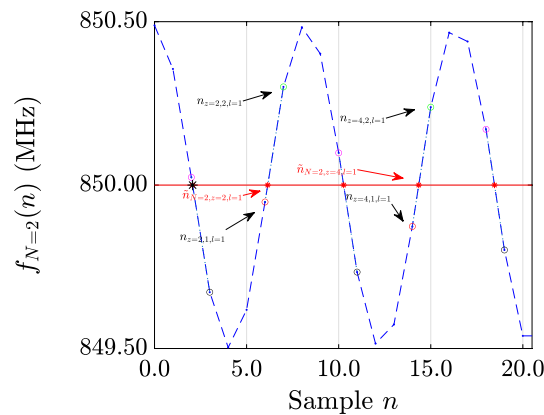


Fig. 2 Instantaneous frequency $f_{N=2}$ sampled with $N_M = 4.1$ showing even zero crossings ($z = 2$ and $z = 4$): samples just before and just after the second zero crossing, $n_{z=2,1,l=1}, n_{z=2,2,l=1}$, second zero crossing sample estimate $\tilde{n}_{N=2,z=2,l=1}$, samples just before and just after the fourth zero crossing, $n_{z=4,1,l=1}, n_{z=4,2,l=1}$, fourth zero crossing sample estimate $\tilde{n}_{N=2,z=4,l=1}$. The red “x” indicate the estimated zero crossings obtained by linear interpolation between the sample values just before and just after the zero crossings

Table 2 Notation (Figs. 1 and 2)

Sample n	$n_{z,1,l}$	Figure
2	$n_{z=1,1,l=1}$	Figure 1
3	$n_{z=1,2,l=1}$	Figure 1
6	$n_{z=2,1,l=1}$	Figure 2
7	$n_{z=2,2,l=1}$	Figure 2
10	$n_{z=3,1,l=1}$	Figure 1
11	$n_{z=3,2,l=1}$	Figure 1
14	$n_{z=4,1,l=1}$	Figure 2
15	$n_{z=4,2,l=1}$	Figure 2

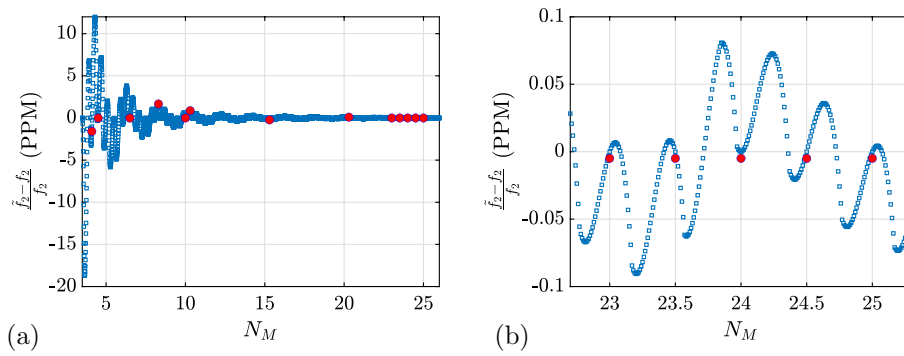


Fig. 3 Relative error in the weak signal frequency $\frac{\hat{f}_{2,z,l} - f_{2,z,l}}{f_2}$ in tier l as a function of N_M for estimates obtained with first (downward) zero crossing ($z_{l=1} = 1$) and third (downward) zero crossing ($z_{l=1} = 3$) in tier $l = 1$; **a** N_M from 3.5 to 26.0; **b** N_M from 22.7 to 25.3. Red dots are values of relative error in weak signal frequency estimates obtained using linear interpolation to estimate first and third downward zero crossings

$$f_{N=2,l}(n) = f_1 + R_{2,l} \Delta f_{21,l} \cos(2\pi \Delta f_{21,l} n T_{s,l}), \quad (31)$$

$$= f_1 + R_{2,l} \Delta f_{21,l} \cos\left(\pi n \frac{1}{N_M}\right). \quad (32)$$

The number of samples $N_{f,l}$ in one period of the instantaneous frequency in tier l is the ratio of the period $T_{N=2,l}$ to the sample period $T_{s,l}$,

$$N_{f,l} = \frac{T_{N=2,l}}{T_{s,l}}, \quad (33)$$

$$= 2N_M. \quad (34)$$

In a period $\lfloor 2N_M \rfloor$, the sample n is $0 \leq n \leq \lfloor 2N_M \rfloor - 1$ (Figs. 1 and 2).

We consider the z_l th zero crossing ($z_l \geq 1$) in tier l . With the oscillatory behavior of the instantaneous frequency, the odd zero crossings are downward zero crossings ($z_l = 1, 3, \dots$), and the even zero crossings are upward zero crossings ($z_l = 2, 4, \dots$).

We set the instantaneous frequency equal to f_1 and determine estimates of two downward (upward) zero crossings $\{\tilde{n}_{N=2,z,l}, \tilde{n}_{N=2,z+2,l}\}$,

$$\tilde{n}_{N=2,z,l} = n_{z,1,l} + \left(\frac{1}{f(n_{z,2,l}) - f(n_{z,1,l})} \right) (f_1 - f(n_{z,1,l})), \quad (35)$$

$$\tilde{n}_{N=2,z+2,l} = n_{z+2,1,l} + \left(\frac{1}{f(n_{z+2,2,l}) - f(n_{z+2,1,l})} \right) (f_1 - f(n_{z+2,1,l})), \quad (36)$$

An estimate of the sample period $\tilde{N}_{N=2,z,l}$ is

$$\tilde{N}_{N=2,z,l} = \tilde{n}_{N=2,z+2,l} - \tilde{n}_{N=2,z,l}. \quad (37)$$

In each tier l , the weak signal frequency estimate $\hat{f}_{2,z,l}$ and weak signal amplitude estimate $\hat{R}_{2,z,l}$ are calculated from the zero crossing pair, $\{z, z + 2\}$ in tier l as

$$\tilde{f}_{2,z,l} = f_1 + \frac{2N_M(f_2 - f_1)}{\tilde{n}_{N=2,z+2,l} - \tilde{n}_{N=2,z,l}}, \quad (38)$$

$$\tilde{R}_{2,z,l} = -\cos[2\pi(\Delta f_{21,z,l})T_{s,l}\tilde{n}_{N=2,z,l}]. \quad (39)$$

The error $\delta f_{2,z,l}$ ($\delta R_{2,z,l}$) is the difference between the weak signal frequency estimate $\tilde{f}_{2,z,l}$ (weak signal amplitude estimate $\tilde{R}_{2,z,l}$) and true value of the weak signal frequency $f_{2,z,l}$ (true value of the weak signal amplitude $R_{2,z,l}$) as,

$$\delta f_{2,z,l} = \tilde{f}_{2,z,l} - f_{2,z,l}, \quad (40)$$

$$\delta R_{2,z,l} = \tilde{R}_{2,z,l} - R_{2,z,l}. \quad (41)$$

The relative error $\left(\frac{\delta f_{2,z,l}}{f_{2,z,l}}\right)\%$ ($\left(\frac{\delta R_{2,z,l}}{R_{2,z,l}}\right)\%$) of the weak signal frequency (amplitude) is the ratio of the error $\delta f_{2,z,l}$ ($\delta R_{2,z,l}$) to the true value of the weak signal frequency $f_{2,z,l}$ ($R_{2,z,l}$),

$$\left(\frac{\delta f_{2,z,l}}{f_{2,z,l}}\right)\% = \left(\frac{\tilde{f}_{2,z,l} - f_{2,z,l}}{f_{2,z,l}}\right) \times 100\%, \quad (42)$$

$$\left(\frac{\delta R_{2,z,l}}{R_{2,z,l}}\right)\% = \left(\frac{\tilde{R}_{2,z,l} - R_{2,z,l}}{R_{2,z,l}}\right) \times 100\%. \quad (43)$$

4.1 Odd zero crossings

The first (downward) zero crossing occurs between two samples $n_{z=1,1,l=1}$ and $n_{z=1,2,l=1}$ just before and just after the $(z = 1)^{st}$ zero crossing in tier $l = 1$ as,

$$n_{z=1,1,l=1} = \left\lfloor \frac{1}{4}N_f \right\rfloor, \quad (44)$$

$$n_{z=1,2,l=1} = \left\lfloor \frac{1}{4}N_f \right\rfloor + 1. \quad (45)$$

For the z_l th odd zero crossing, the instantaneous frequencies $f(n_{z,1,l})$ and $f(n_{z,2,l})$ at the points $\{n_{z,1,l}, n_{z,2,l}\}$ just before and just after the zero crossing are,

$$f(n_{z,1,l}) = f_1 + R_{2,l}\Delta f_{21,l} \cos\left(\frac{\pi\left(\left\lfloor \frac{1}{2}N_M \right\rfloor + \left(\frac{z_l-1}{2}\right)\lfloor 2N_M \rfloor\right)}{N_M}\right), \quad (46)$$

$$f(n_{z,2,l}) = f_1 + R_{2,l}\Delta f_{21,l} \cos\left(\frac{\pi\left(\left\lfloor \frac{1}{2}N_M \right\rfloor + \left(\frac{z_l-1}{2}\right)\lfloor 2N_M \rfloor + 1\right)}{N_M}\right), \quad (47)$$

An estimate $\tilde{n}_{N=2,z,l}$ of the sample at the z th odd zero crossing is

$$\tilde{n}_{N=2,z,l} = \left\lfloor \frac{1}{2}N_M \right\rfloor + \left(\frac{z_l - 1}{2} \right) \lfloor 2N_M \rfloor \tag{48}$$

$$+ \left(\frac{1}{\cos \left(\frac{\pi \left(\left\lfloor \frac{1}{2}N_M \right\rfloor + \left(\frac{z_l - 1}{2} \right) \lfloor 2N_M \rfloor + 1 \right)}{N_M} \right)} - \cos \left(\frac{\pi \left(\left\lfloor \frac{1}{2}N_M \right\rfloor + \left(\frac{z_l - 1}{2} \right) \lfloor 2N_M \rfloor \right)}{N_M} \right)} \right) \times \tag{49}$$

$$\times \cos \left(\frac{\pi \left(\left\lfloor \frac{1}{2}N_M \right\rfloor + \left(\frac{z_l - 1}{2} \right) \lfloor 2N_M \rfloor \right)}{N_M} \right). \tag{50}$$

Sample estimates $\tilde{n}_{N=2,z=1,l}$ and $\tilde{n}_{N=2,z=3,l}$ are substituted in Eqs. 37–43 to obtain weak signal parameter estimates and relative errors.

4.2 Even zero crossings

A similar procedure is used to obtain sample estimates for the even zero crossings. The second (upward) zero crossing occurs between two samples $n_{z=2,1,l}$ and $n_{z=2,2,l}$ just before and just after the ($z = 2$)th zero crossing,

$$n_{z=2,1,l} = \left\lfloor \frac{1}{4}N_f \right\rfloor + \lfloor N_M \rfloor, \tag{51}$$

$$n_{z=2,2,l} = \left\lfloor \frac{1}{4}N_f \right\rfloor + 1 + \lfloor N_M \rfloor. \tag{52}$$

For the z th even zero crossing, the instantaneous frequencies at the points $\{n_{z,1}, n_{z,2}\}$ just before and just after the zero crossing z_l in tier l are,

$$f(n_{z,1,l}) = f_1 + R_{2,l} \Delta f_{21,l} \cos \left(\frac{\pi \left(\left\lfloor \frac{1}{2}N_M \right\rfloor + \lfloor N_M \rfloor + \left(\frac{z_l - 1}{2} \right) \lfloor 2N_M \rfloor \right)}{N_M} \right), \tag{53}$$

$$f(n_{z,2,l}) = f_1 + R_{2,l} \Delta f_{21,l} \cos \left(\frac{\pi \left(\left\lfloor \frac{1}{2}N_M \right\rfloor + \lfloor N_M \rfloor + \left(\frac{z_l - 1}{2} \right) \lfloor 2N_M \rfloor + 1 \right)}{N_M} \right), \tag{54}$$

An estimate $\tilde{n}_{N=2,z=2,l}$ of the sample at the z th even zero crossing is

$$\tilde{n}_{N=2,z=2,l} = \left\lfloor \frac{1}{2}N_M \right\rfloor + \lfloor N_M \rfloor + \lfloor 2N_M \rfloor \tag{55}$$

$$+ \left(\frac{1}{\cos \left(\frac{\pi \left(\left\lfloor \frac{1}{2} N_M \right\rfloor + \lfloor 2N_M \rfloor + \lfloor N_M \rfloor + 1 \right\rfloor}{N_M} \right)} \right) - \cos \left(\frac{\pi \left(\left\lfloor \frac{1}{2} N_M \right\rfloor + \lfloor 2N_M \rfloor + \lfloor N_M \rfloor \right)}{N_M} \right)} \right) \times \quad (56)$$

$$\times \cos \left(\frac{\pi \left(\left\lfloor \frac{1}{2} N_M \right\rfloor + \lfloor N_M \rfloor + \lfloor 2N_M \rfloor \right)}{N_M} \right). \quad (57)$$

The sample estimates $\tilde{n}_{N=2,z=2,l}$ and $\tilde{n}_{N=2,z=4,l}$ are substituted in Eqs. 37–43 to obtain weak signal parameter estimates and relative errors.

5 Weak RF signal estimation process with dynamic sampling for $N = 2$ simultaneous signals

We start by revisiting a three-tier weak signal estimation process for $N = 2$ simultaneous signals [33–39]. The parameter values are $R_1 = 1$, $R_{2,1} = R_{2,2} = R_{2,3} = 0.01$, $f_1 = 850$ MHz, $f_{2,l=1} = 855$ MHz, $f_{2,l=2} = 851$ MHz, $f_{2,l=3} = 852$ MHz, with three tiers have duration $1 \mu\text{s}$ ($l = 1$), $4 \mu\text{s}$ ($l = 2$) and $1.5 \mu\text{s}$ ($l = 3$), with $\phi_k(t) = \phi_k(n) = 0$. These values are substituted in Eq. 32 to obtain the instantaneous frequency $f_{N=2}(t)$ shown in Fig. 4.

The zero crossing error decreases as sample rate increases. The results in Fig. 4 show that the zero crossing error is less than 5×10^{-15} s for sample rate $f_s = 5.2$ GSPS, less than 1×10^{-13} s for $f_s = 1$ GSPS, and less than 4×10^{-11} s for $f_s = 65$ MSPS, respectively.

Weak signal parameter estimates $\tilde{f}_{2,z,l}$ and $\tilde{R}_{2,z,l}$ are obtained in each tier l and are shown in Fig. 5a and b for sample rates of 5.2 GSPS and 1 GSPS, respectively. The relative errors $\left(\frac{\delta f_{2,z,l}}{f_{2,z,l}} \right) \%$ and $\left(\frac{\delta R_{2,z,l}}{R_{2,z,l}} \right) \%$ in the weak signal parameter estimates are shown in Fig. 5c and d, for $f_s = 5.2$ GSPS and $f_s = 1$ GSPS, respectively.

The relative errors of the estimates of the weak signal parameters are shown in Fig. 6 as functions of N_M . The results show the relative errors for the weak signal parameters, respectively, for $N_M = 2$ to $N_M = 5$, 5–15, and 15–50.

We note specifically that the results in Fig. 6 show that the relative error in the estimates of the weak signal frequency and amplitude takes on zero value for some values of N_M . The results show that as N_M increases, then the relative error in the weak signal parameter estimates tend to decrease. At the same time, the results show that lower error values are obtained at lower sample rates compared with error rates achieved when the sample rates take on higher value, since the error rate oscillates as a function of N_M .

The results in Fig. 6 show that the relative errors of the weak signal parameter estimates exhibit a behavior similar to that of an underdamped system. We model the upper and lower bound exponential decay envelopes $f_{2,\text{envelope}}$ and $R_{2,\text{envelope}}$ for the decaying behavior of the relative errors of the weak signal parameters in Fig. 6,

$$f_{2,\text{envelope}} = \pm A_f e^{-\zeta_f \omega_{t,f} n}, \quad (58)$$

$$R_{2,\text{envelope}} = \pm A_R e^{-\zeta_R \omega_{t,R} n}, \quad (59)$$

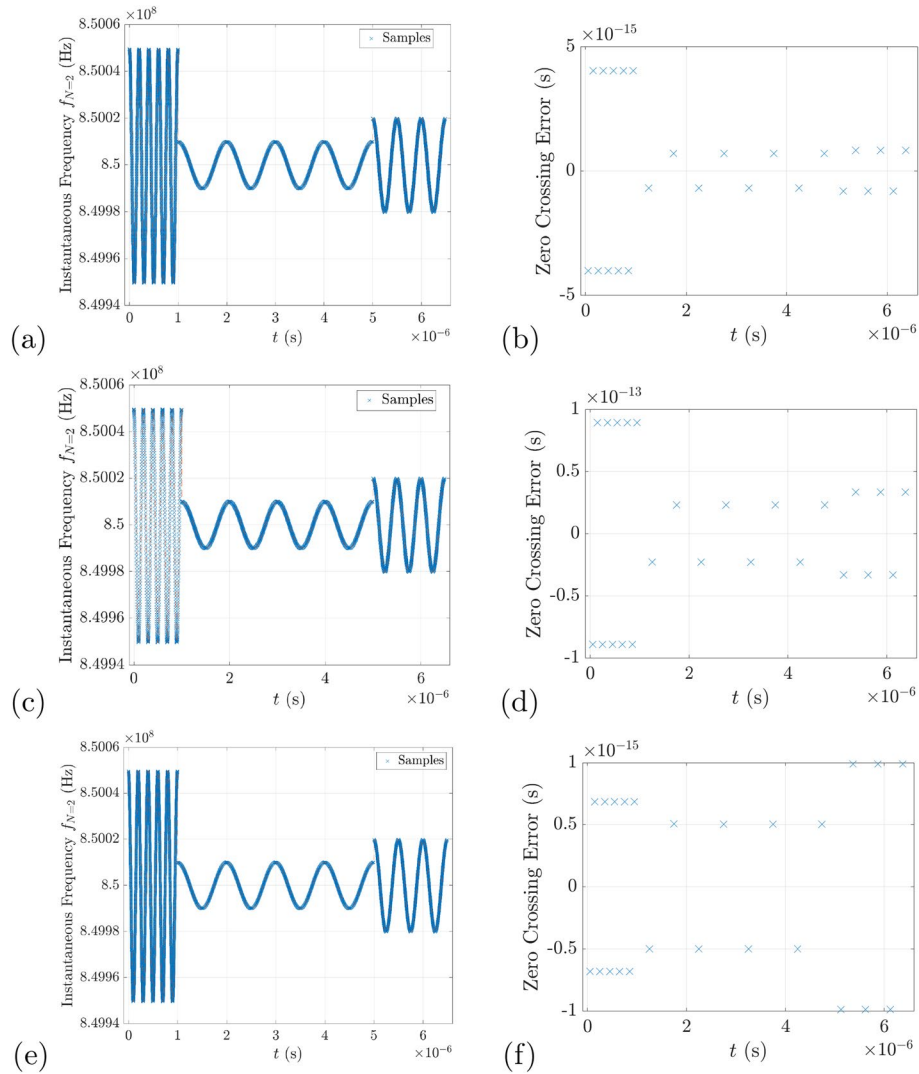


Fig. 4 Instantaneous frequency $f_{N=2}$ sampled at (a) 5.2 GSPS; (c) 1 GSPS, (e) 65 MSPS with zero crossing error (blue "x") for (b) 5.2 GSPS; (d) 1 GSPS; (f) 65 mps

where A_f and A_R represent the initial amplitudes of the weak signal parameter estimates; $\omega_{t,f} = \frac{1}{2\pi T_f}$ and $\omega_{t,R} = \frac{1}{2\pi T_R}$ represent damping factor frequencies; T_f and T_R are the corresponding periods for the weak signal parameters; and ζ_f and ζ_R represent damping factors, where

$$\zeta_f = \frac{\delta_f}{\sqrt{\delta_f^2 + 4\pi^2}}, \quad (60)$$

$$\zeta_R = \frac{\delta_R}{\sqrt{\delta_R^2 + 4\pi^2}}, \quad (61)$$

and where δ_f and δ_R represent the logarithmic decrements and are calculated using successive peaks in the weak signal parameters,

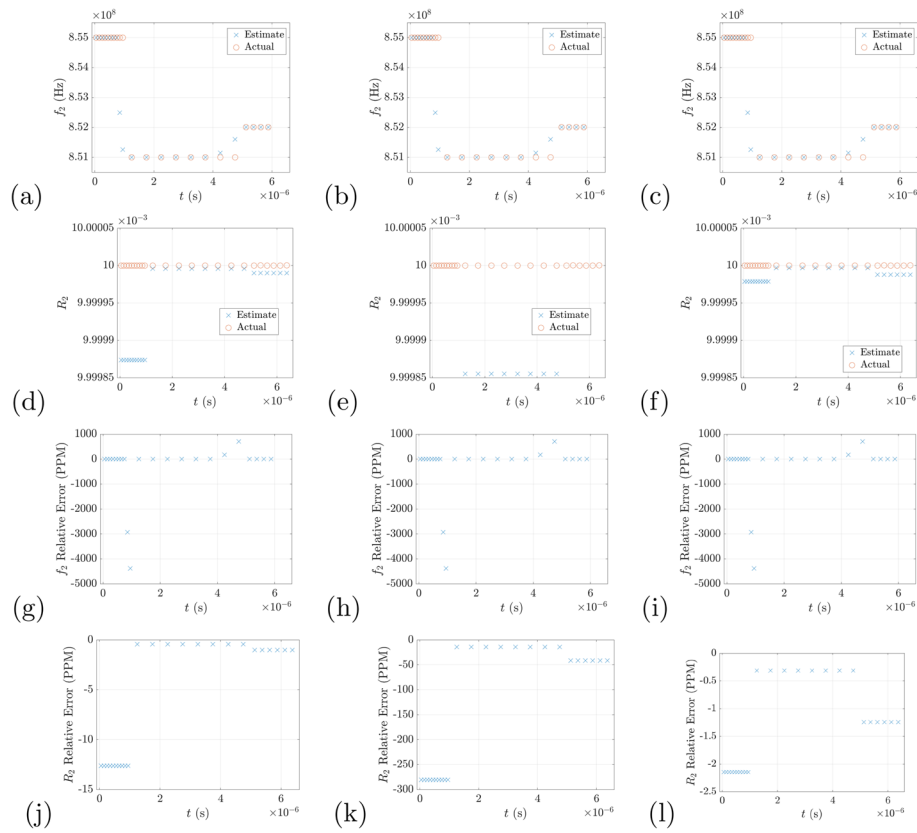


Fig. 5 Estimates (blue “x”) with actual values (red open circles) using $f_{N=2}$ sampled at 5.2 GSPS for a strong signal with $f_1 = 850$ MHz with weak signal **(a)** frequency and **(d)** amplitude; Relative error in estimates of weak signal **(g)** frequency and **(j)** amplitude; sampled at 1 GSPS for weak signal **(b)** frequency and **(e)** amplitude; Relative error in estimates of weak signal **(h)** frequency and **(k)** amplitude; sampled at 65 msps for weak signal **(c)** frequency and **(f)** amplitude; Relative error in estimates of weak signal **(i)** frequency and **(l)** amplitude

$$\delta_f = \ln \left(\frac{x_{0,f}}{x_{1,f}} \right), \quad (62)$$

$$\delta_R = \ln \left(\frac{x_{0,R}}{x_{1,R}} \right). \quad (63)$$

In these expressions, $x_{0,f}$ and $x_{1,f}$ represent amplitudes of two successive peaks in the relative error of the weak signal frequency as a function of N_M , and $x_{0,R}$ and $x_{1,R}$ represent two successive peaks in the relative error of the weak signal amplitude estimate. For Fig. 6d, Eq. 59 is solved to obtain the value of A_R at $n = 5$.

Figure 7a and b shows estimates of zero crossings and the difference between the estimates of the zero crossings and actual zero crossings as a function of Nyquist multiple N_M $N = 2$ simultaneous signals where the strong signal frequency $f_1 = 850$ MHz; the strong signal amplitude $R_1 = 1$; the weak signal frequency $f_2 = 855$ MHz; and the weak signal amplitude $R_2 = 0.01$ (Fig. 8).

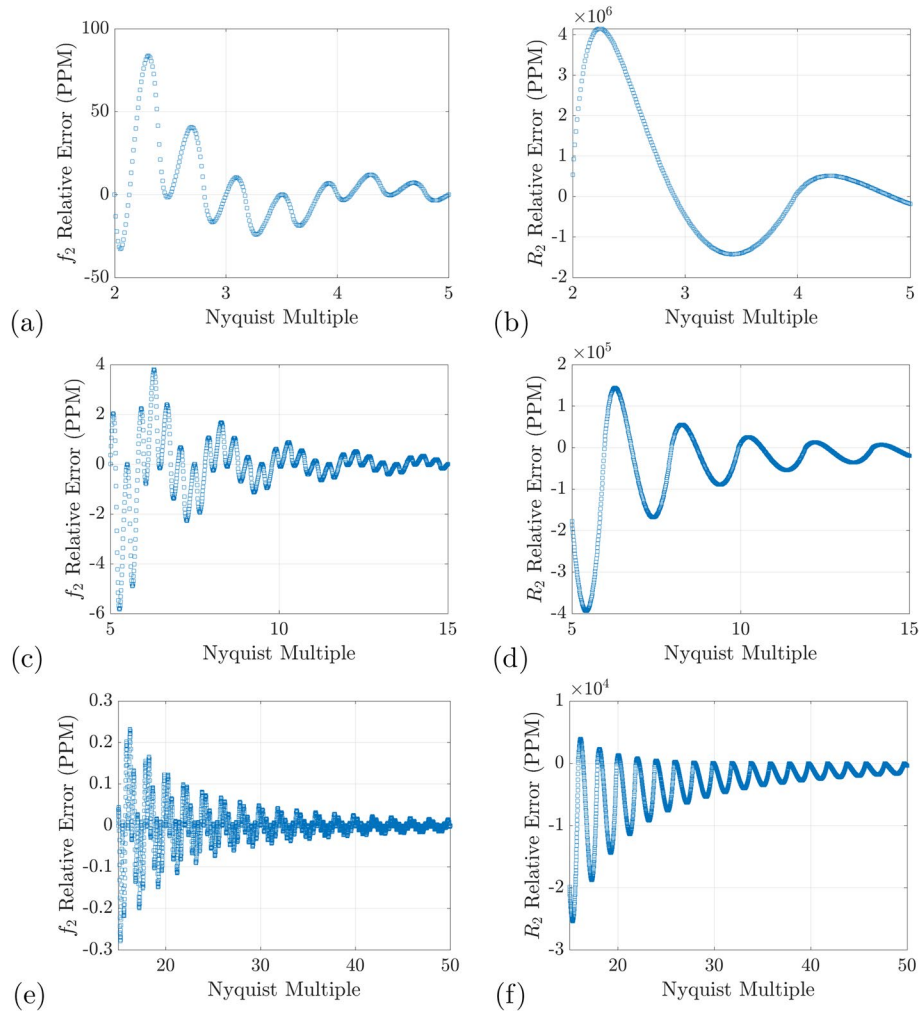


Fig. 6 Relative error in f_2 for N_M (a) 2–5, (c) 5–15, (e) 15–50; and relative error in R_2 for N_M (b) 2–5, (d) 5–15, (f) 15–50

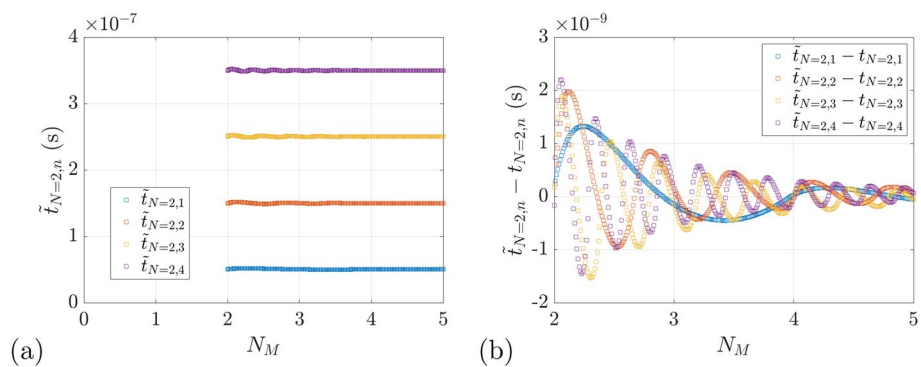


Fig. 7 **a** Estimates of zero crossings and **b** difference between the estimates of the zero crossings and actual zero crossings as a function of Nyquist multiple N_M for $N = 2$ simultaneous signals with strong signal frequency $f_1 = 850$ MHz; strong signal amplitude $R_1 = 1$; weak signal frequency $f_2 = 855$ MHz; and weak signal amplitude $R_2 = 0.01$

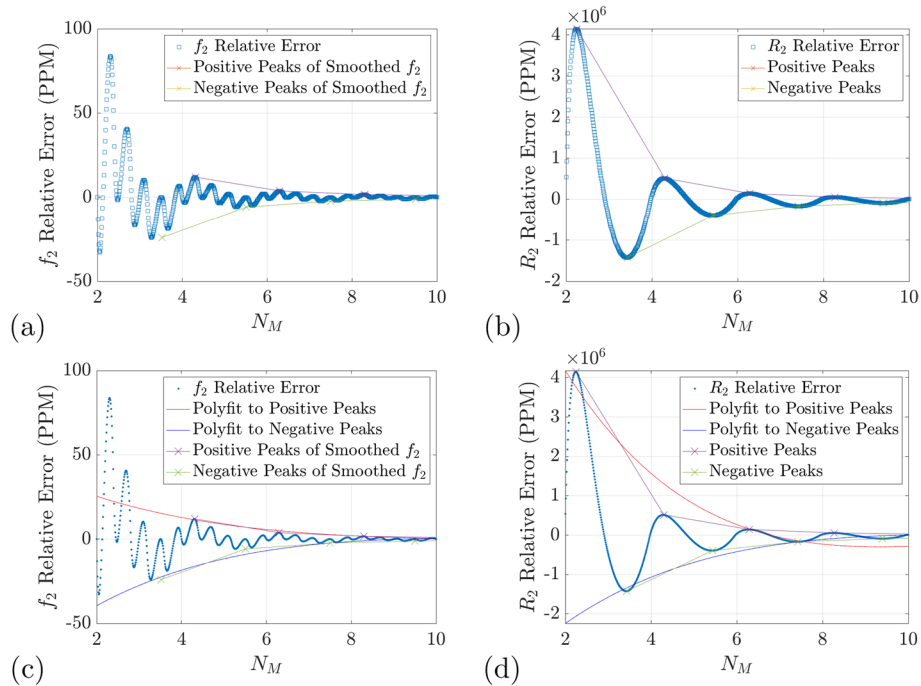


Fig. 8 Peaks in (a) relative error of the weak signal frequency and peaks in the (b) weak signal amplitude; Polyfits to smoothed peaks in (c) relative error of the weak signal frequency and peaks in the (d) weak signal amplitude

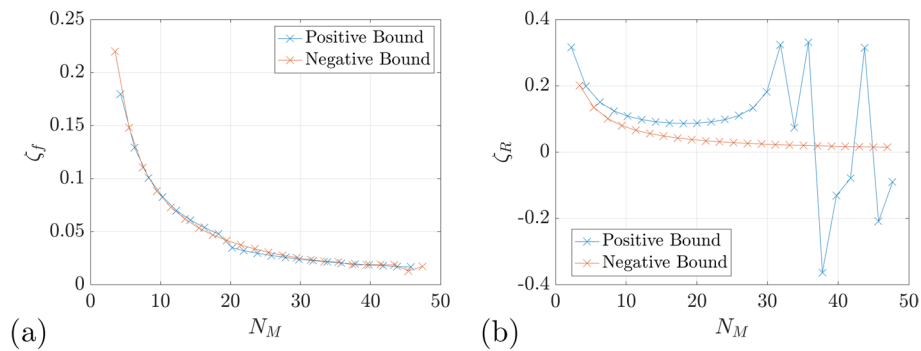


Fig. 9 Damping factor ζ_f (a) from Fig. 6a, c, e, Damping factor ζ_R (b) from Fig. 6b, d, f

Values for the quantities $\zeta_R \omega_{t,R}$ at each N_M are obtained by solving Eq. 59 at two points in time where the peaks occur, such as for $n = 6.29$ and $n = 8.27$, respectively, which are the values of N_M for the first two peaks that take on positive values in Fig. 6d.

Figure 9a and b show the extracted values of the damping factors for weak signal parameters f_2 and R_2 as functions of N_M (from $N_M = 2$ to $N_M = 50$) for the weak signal frequency and amplitude, respectively. The results show that the damping factor changes as a function of N_M for the relative errors of the weak signal parameters estimates.

The results in Fig. 9a show that the damping factor for the weak signal frequency relative error tends to decrease as N_M increases. The results also show that the relative

error of the weak signal frequency estimate exhibits similar values of the damping factors for the upper bound exponential decay function compared with the damping factors of the lower bound exponential decay function.

The results in Fig. 9b show that the damping factor for the weak signal amplitude relative error also changes as a function of N_M . The results show that the damping factor for the lower (negative) bound tends to decrease as N_M increases. The results also show that the damping factor for the upper (positive) bound tends to decrease as N_M increases from $N_M = 2$ to $N_M = 30$, and then the damping factor takes on relatively large oscillating values.

Determining the dependence of the bounds in the relative error of the weak signal parameters as functions of N_M provides a capability. This capability provides the ability to extract the minimum value of N_M to obtain a specified desired relative error (and therefore, to extract the corresponding minimum sample rate). Indeed, the results show that there actually exists a value of N_M to obtain a zero relative error.

The results also show that the relative error of the weak signal amplitude R_2 tends to remain larger than the relative error for the weak signal frequency for large values of N_M , and even for values as high as $N_M = 50$. Selecting such a large value of the sample rate to improve an estimate of the weak signal amplitude R_2 may be unachievable.

Another approach is to use the oscillatory nature of the relative error as a function of N_M to our advantage and determine the values of N_M for which the relative error takes on a zero value. There exist multiple values of f_s for which the relative error in the weak signal frequency estimate takes on a value of zero. As an example, when $N_M = 24$, as shown in the marker point in the box in Fig. 10a, the relative error in the weak signal frequency estimate is zero. The results in Fig. 10 show that when $N_M = 24$, the relative error of the weak signal amplitude estimate is 427.155 PPM, as shown in Fig. 10b.

5.1 Dynamic sampling

Figure 11 shows a three-tier weak signal estimation process with dynamic sampling and $N_M = 24$. We set $R_1 = 1$, $R_{2,1} = R_{2,2} = R_{2,3} = 0.01$, $f_1 = 850$ MHz, $f_{2,l=1} = 855$ MHz, $f_{2,l=2} = 851$ MHz, $f_{2,l=3} = 852$ MHz. The tier durations are set to $\Delta l_1 = 1$ μ s, $\Delta l_2 = 4$ μ s and $\Delta l_3 = 1.5$ μ s, respectively. These values are chosen to allow for a direct comparison for each tier with the results of our prior case study. In this example, the analysis assumes to have no prior knowledge of the weak signal parameter values. The value of the sample

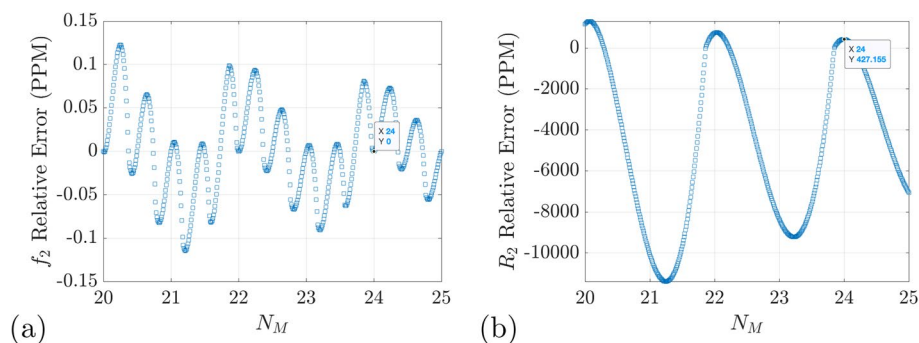


Fig. 10 Relative error (PPM) for **a** f_2 and **b** R_2

rate is adjusted every three zero crossings. The initial sample rate $f_{s,0}$ is set to the value $f_{s,0} = 65$ MSPS. The parameters are substituted in Eq. 32 for each tier l to obtain the instantaneous frequency. Figure 11a shows the instantaneous frequency of the three-tier process. The zero crossings are estimated using linear interpolation and are shown in Fig. 11b. The zero crossing error in the instantaneous frequency is shown in Fig. 11c.

Estimated zero crossings are obtained from Fig. 11b. Then, estimates of the weak signal parameters are extracted and shown in Fig. 12a and b, respectively. These results show that the error is reduced in each tier and that the error is larger during the time in each transition from one tier to the subsequent tier. The relative error for the weak signal parameter estimates $f_{2,l}$ and $R_{2,l}$ are shown in Fig. 12c and d, respectively. Significantly, the results in Fig. 12 show that the relative error for the weak signal frequency estimates are nearly zero in each tier except at the two points in time prior to and three points in time after the transition from one tier to the next. In summary, the results in Fig. 12c and d show that changing the sample rate in each tier successfully reduces the zero crossing error to zero.

6 Weak 5G simultaneous signals with a strong signal at 3950 MHz and a weak signal at 3955 MHz

In this section, we discuss approaches to estimating weak 5G signal parameters for a weak 5G signal in the presence of a strong signal. Public awareness of 5G signals is very extensive as a result of its deployment in consumer electronics worldwide. Weak 5G signals may arise due to large “distance from the nearest cell tower, physical obstructions, and network congestion, ... physical obstructions like walls” [41].

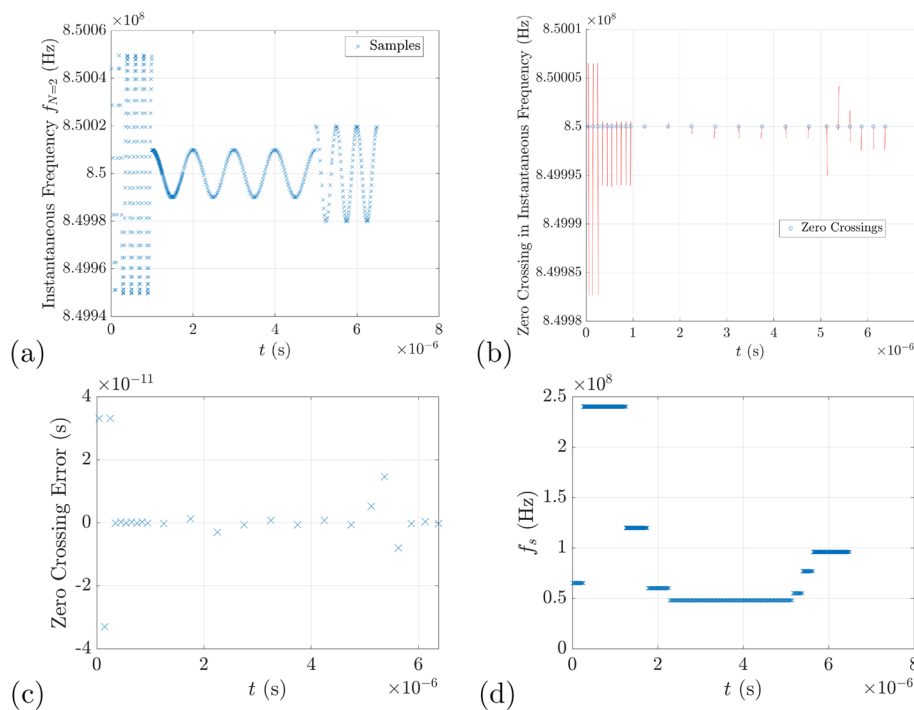


Fig. 11 Dynamic sampling with $N_M = 24$ and **a** sampled instantaneous frequency, **b** zero crossings, **c** zero crossing error, **d** dynamic sampling rate f_s with $N_M = 24$ and sample rate f_s in a three-tier weak signal estimation process

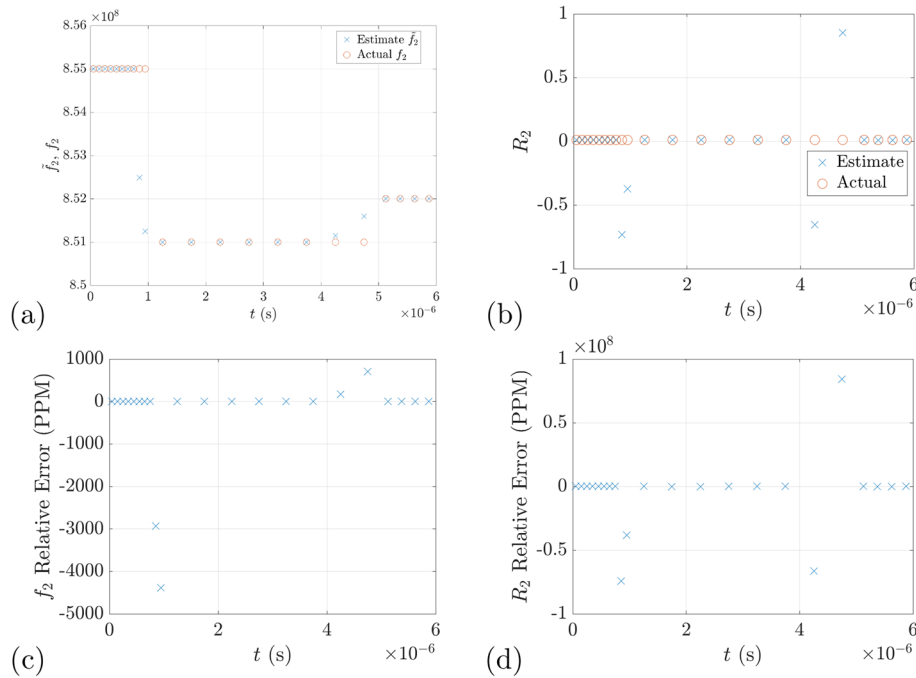


Fig. 12 Dynamic sampling with $N_M = 24$ and weak signal parameter estimates (blue “x”) and actual values (open circles) using dynamic multirate sampling: **a** weak signal frequency f_2 ; **b** weak signal amplitude R_2 . Relative error in estimates of weak signal **c** frequency and **d** amplitude

Thompson [41] discusses ways for the consumer to “troubleshoot” weak 5G signals. Rowe and Luo and Zhang [42, 43] discuss 5G signals and signal processing of 5G signals.

We consider two simultaneous 5G signals. The strong signal frequency is $f_1 = 3950$ MHz, and the weak signal is 3955 MHz. Figure 13a–h shows the instantaneous frequency $f_{N=2}$ as a function of time (a); estimates of zero crossings $\tilde{t}_{N=2,n}$ as a function of Nyquist multiple N_M (b); difference between estimates of zero crossings and actual zero crossings $\tilde{t}_{N=2,n} - t_{N=2,n}$ as a function of N_M (c); estimates of the weak signal amplitude \tilde{R}_2 as a function of N_M (d); estimates of weak signal frequency \tilde{f}_2 as a function of N_M (e); difference between weak signal amplitude estimates and actual weak signal amplitude $\tilde{R}_2 - R_2$ as a function of N_M (f); difference between weak signal frequency estimates and actual weak signal frequency $\tilde{f}_2 - f_2$ as a function of N_M (g); and relative error in the weak signal amplitude $\frac{\tilde{R}_2 - R_2}{R_2}$ as a function of N_M (h).

We next consider three values of the sample rate of the instantaneous frequency for these two simultaneous 5G signals. Figures 14a–g, 15a–g, and 16a–g show results for the case in which the sample rate $f_s = 5.2$ GSPS; $f_s = 1$ GSPS; $f_s = 65$ mspS, respectively, and the strong signal has $f_1 = 3950$ MHz. The figures show the instantaneous frequency with weak signal frequency $f_2 = 3955$ MHz; $f_2 = 3951$ MHz; $f_2 = 3952$ MHz, respectively, in the three tiers (a); zero crossings in the instantaneous frequency as a function of time (b); estimates and actual value of the weak signal amplitude R_2 (c); estimates and actual value of the weak signal frequency f_2 (d); zero crossing error (e); relative error in the weak signal frequency f_2 (f); relative error in the weak signal amplitude R_2 (g).

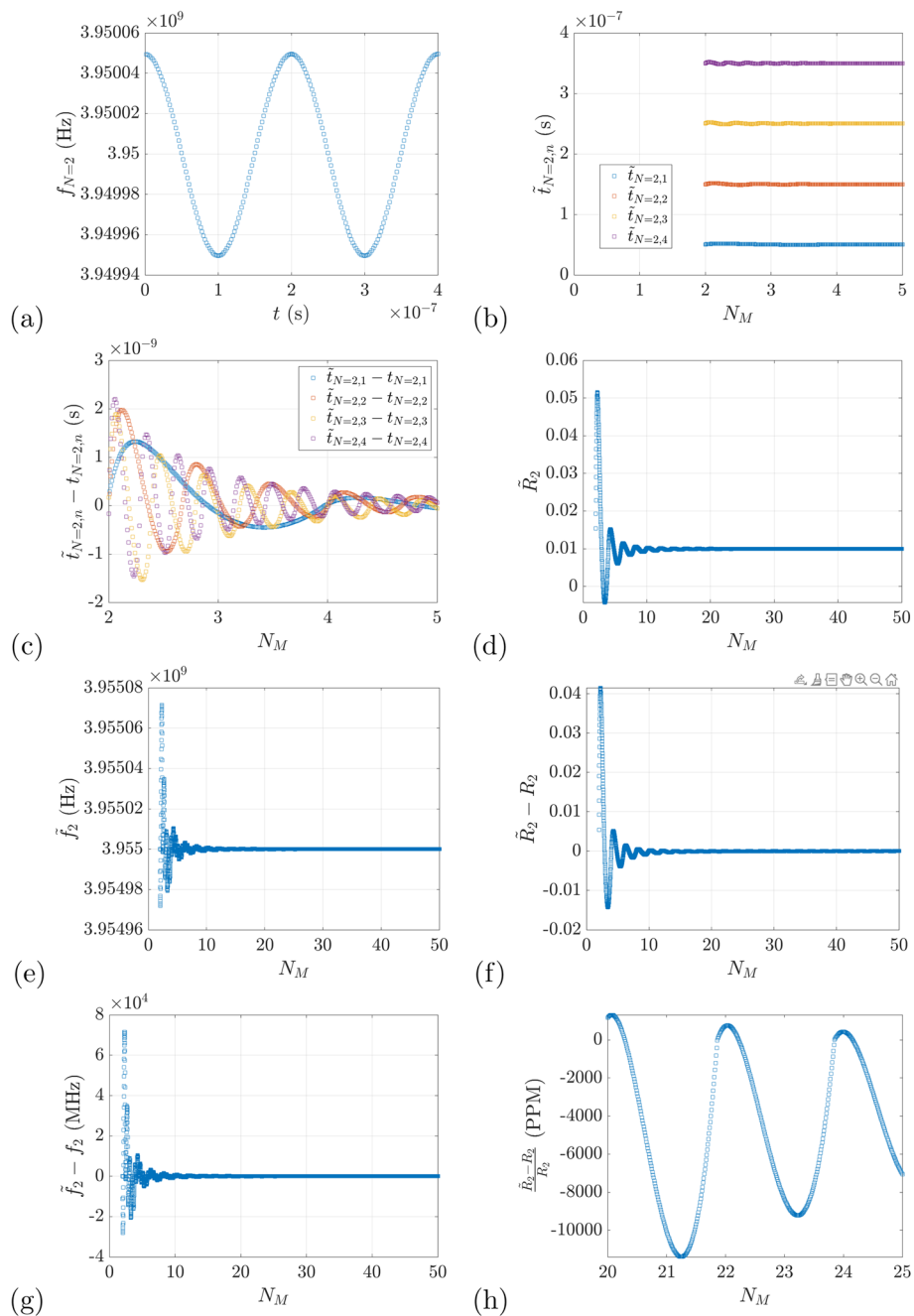


Fig. 13 Strong signal with $f_1 = 3950\text{MHz}$: **a** instantaneous frequency; **b** estimates of zero crossings as a function of Nyquist multiple N_M ; **c** difference between estimates of zero crossings and actual zero crossings as a function of N_M ; **d** estimates of the weak signal amplitude as a function of N_M ; **e** estimates of weak signal frequency as a function of N_M ; **f** difference between weak signal amplitude estimates and actual weak signal amplitude as a function of N_M ; **g** difference between weak signal frequency estimates and actual weak signal frequency as a function of N_M ; **h** relative error in the weak signal amplitude as a function of N_M

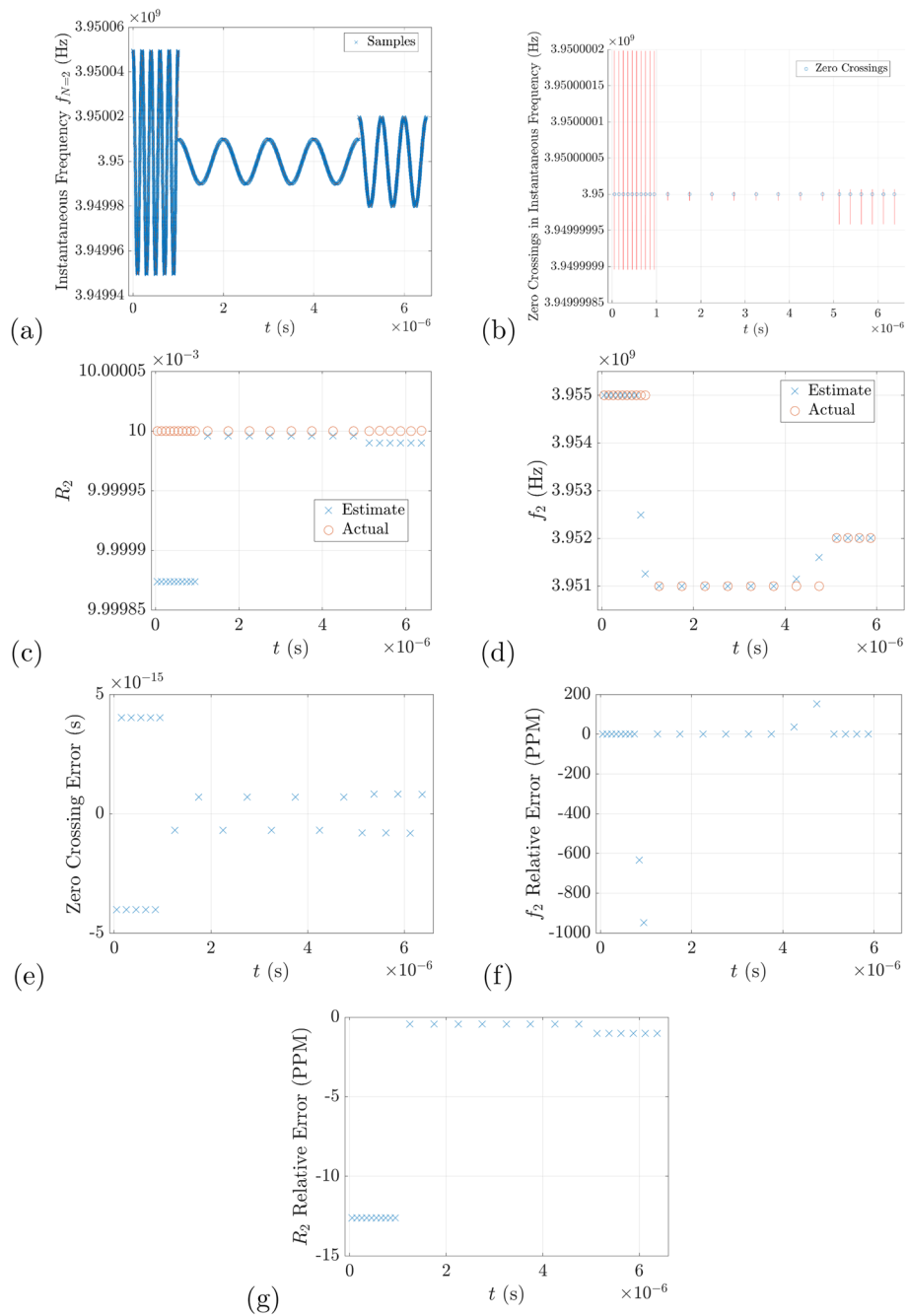


Fig. 14 Sample rate $f_s = 5.2$ GSPS and strong signal with $f_1 = 3950$ MHz; **a** instantaneous frequency with weak signal frequency $f_2 = 3955$ MHz; $f_2 = 3951$ MHz; $f_2 = 3952$ MHz, respectively, in the three tiers; **b** zero crossings in the instantaneous frequency as a function of time; **c** estimates and actual value of the weak signal amplitude R_2 as a function of time; **d** estimates and actual value of the weak signal frequency f_2 ; **e** zero crossing error; **f** relative error in the weak signal frequency f_2 ; **g** relative error in the weak signal amplitude R_2

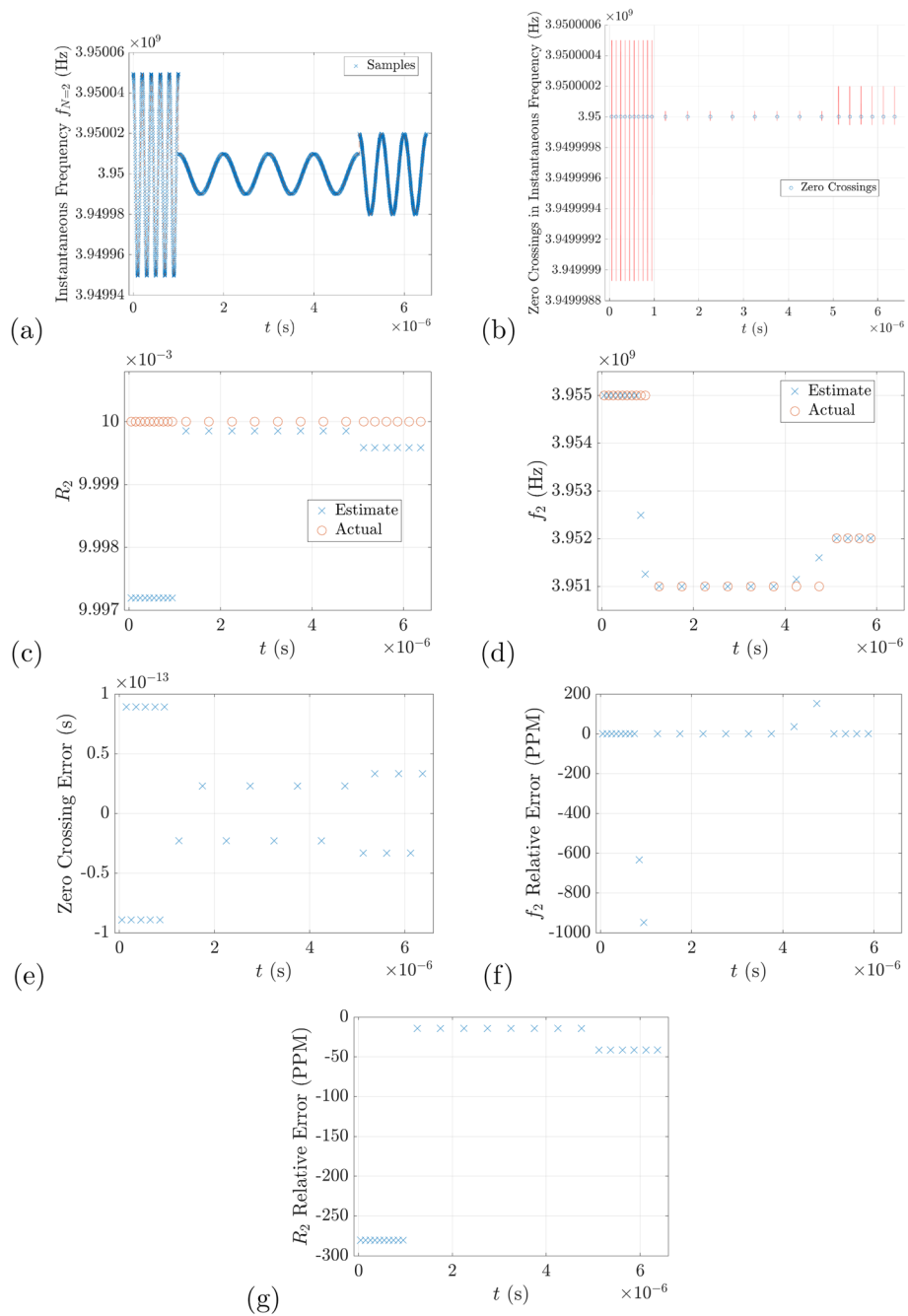


Fig. 15 Sample rate $f_s = 1\text{GSPS}$ and strong signal with $f_1 = 3950\text{MHz}$; **a** instantaneous frequency with weak signal frequency $f_2 = 3955\text{MHz}$; $f_2 = 3951\text{MHz}$; $f_2 = 3952\text{MHz}$, respectively, in the three tiers; **b** zero crossings in the instantaneous frequency as a function of time; **c** estimates and actual value of the weak signal amplitude R_2 ; **d** estimates and actual value of the weak signal frequency f_2 ; **e** zero crossing error; **f** relative error in the weak signal frequency f_2 ; **g** relative error in the weak signal amplitude R_2

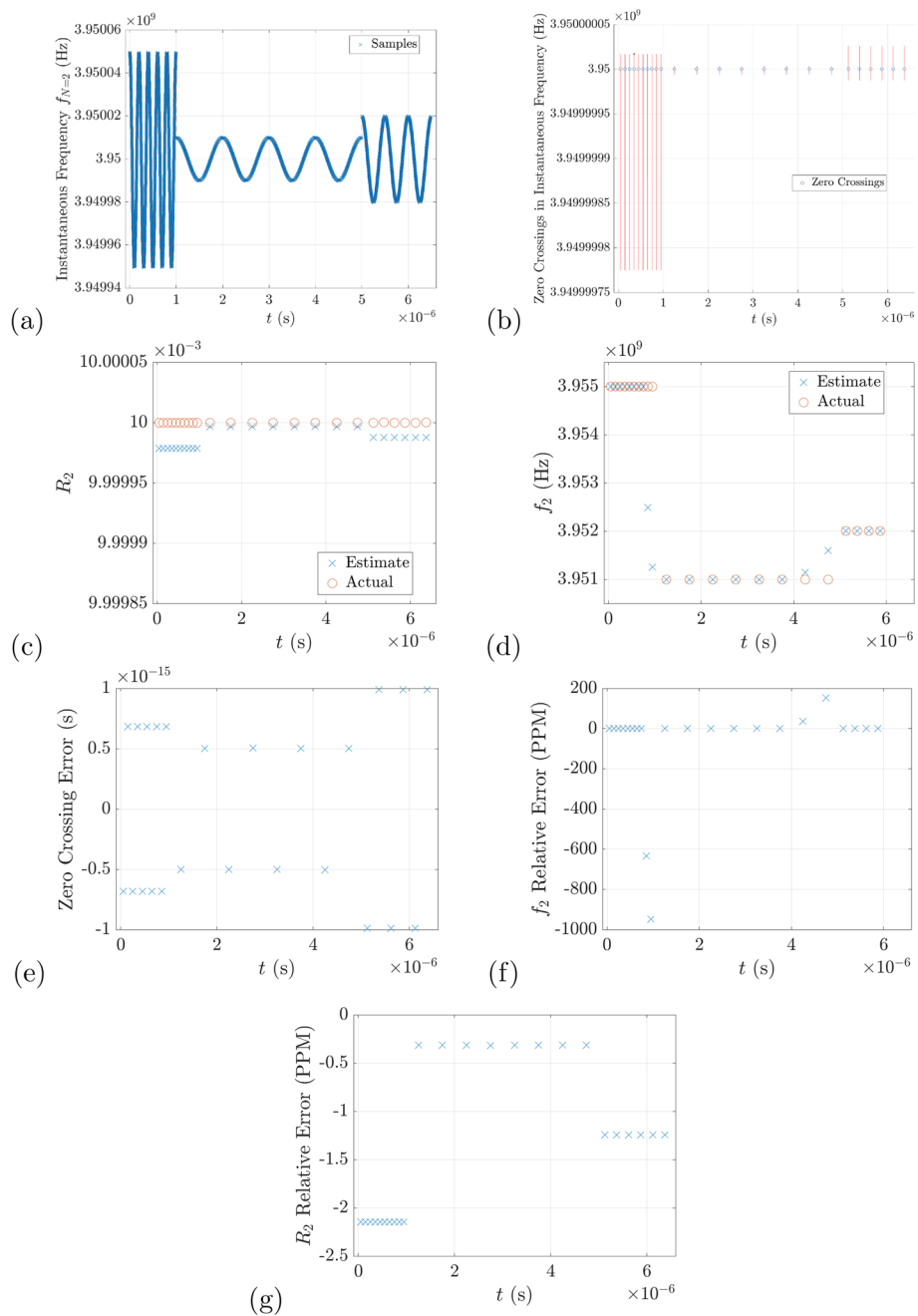


Fig. 16 Sample rate $f_s = 65$ msp/s and strong signal with $f_1 = 3950$ MHz; **a** instantaneous frequency with weak signal frequency $f_2 = 3955$ MHz; $f_2 = 3951$ MHz; $f_2 = 3952$ MHz, respectively, in the three tiers; **b** zero crossings in the instantaneous frequency as a function of time; **c** estimates and actual value of the weak signal amplitude R_2 as a function of time; **d** estimates and actual value of the weak signal frequency f_2 ; **e** zero crossing error; **f** relative error in the weak signal frequency f_2 ; **g** relative error in the weak signal amplitude R_2

We next obtain accurate weak signal frequency estimate for the weak 5G signal using dynamic sampling. Figure 17a–h show the dynamic sampling at 3950 MHz with three tiers where sampling rate f_s changes based on data collected in real time. The figure shows the instantaneous frequency as a function of time (a); the instantaneous frequency with zero crossings (b); estimates and actual weak signal amplitude (c); estimates

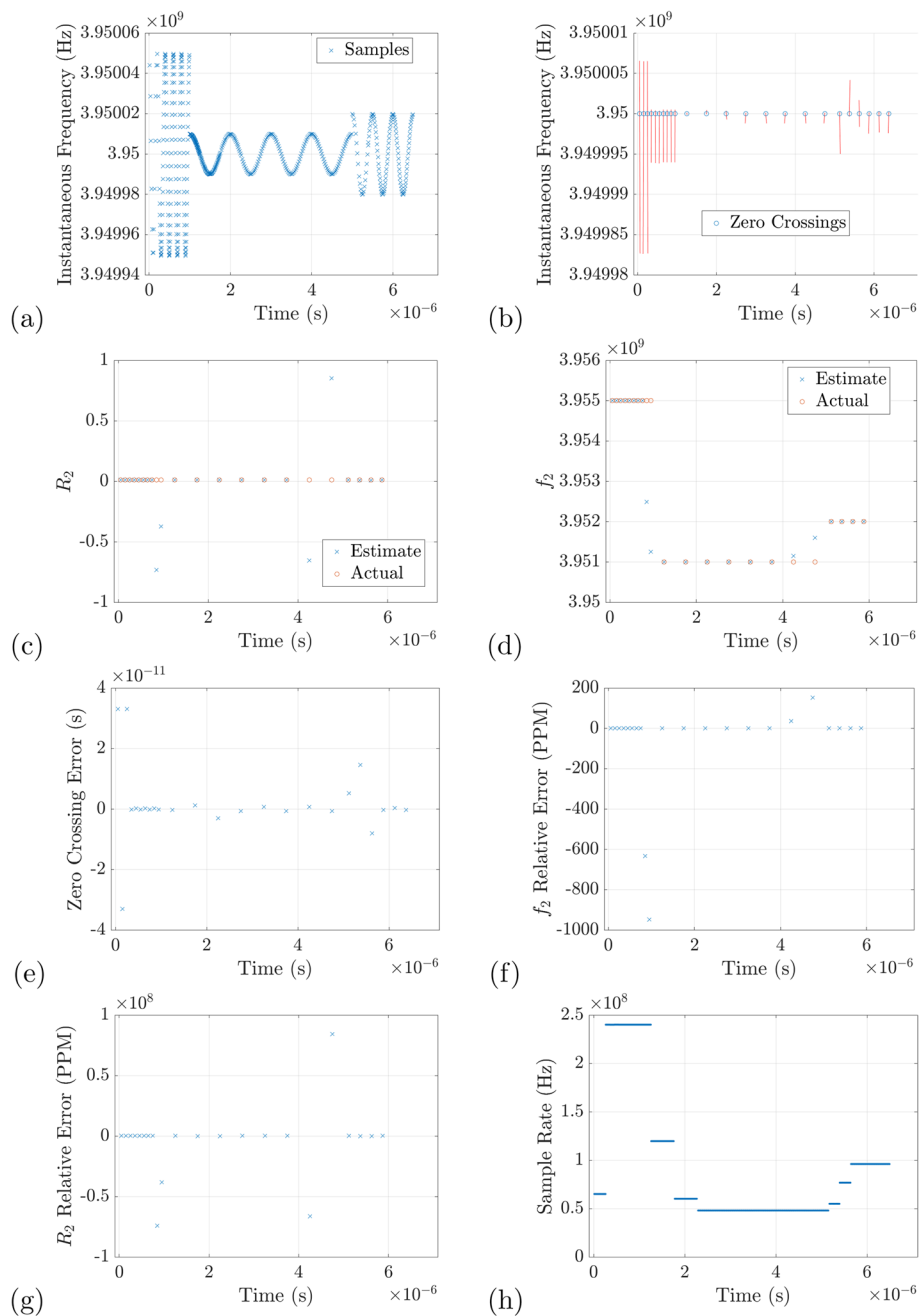


Fig. 17 Dynamic sampling at 3950 MHz with three tiers where sampling rate f_s changes based on data collected in real time: **a** instantaneous frequency as a function of time; **b** instantaneous frequency with zero crossings; **c** estimates and actual weak signal amplitude; **d** estimates and actual weak signal frequency; **e** zero crossing error; **f** relative error in the weak signal frequency estimate; **g** relative error in the weak signal amplitude estimate; **h** sample rate in each tier determined based on data collected in real time

and actual weak signal frequency (d); zero crossing error (e); relative error in the weak signal frequency estimate (f); relative error in the weak signal amplitude estimate (g); sample rate in each tier determined based on data collected in real time (h). The results are summarized in the tables in the next section.

7 Discussion and conclusion

This paper presents results that demonstrate the capability to obtain weak signal parameter estimates with very low relative error in multi-tier weak RF and weak 5G signal parameter estimation processes. The low relative error is achieved in real time with a dynamic sample rate that is $N_M = 24$ times as large as the frequency of the instantaneous frequency. In each tier, the dynamic sample rate takes on a different value thereby providing very small relative error for the weak signal parameter estimates.

Tables 3, 4, 5 shows a comparison of the relative error in the weak signal frequency estimates using $f_s = 5.2$ GSPS shown in Fig. 5g, 1 GSPS in Fig. 5h, and 65 MSPS in Fig. 5i. The results for the relative error for the weak signal frequency estimates are less than 2×10^{-9} PPM for sample rates of 1 GSPS and 5.2 GSPS. For these sample rates, the relative error in the weak signal amplitude ranges from approximately -280 PPM to approximately -0.4 PPM. These values for the relative error in the weak signal amplitude

Table 3 Comparison of weak signal parameter estimates \tilde{f}_2 and \tilde{R}_2 obtained using a dynamic sample rate with estimates obtained using a single sample rate for $N = 2$ simultaneous signals for weak signal parameters $f_{2,l=1} = 855$ MHz, $f_{2,l=2} = 851$ MHz, $f_{2,l=3} = 852$ MHz, and $R_{2,l=1} = R_{2,l=2} = R_{2,l=3} = 0.01$

l	t (μ s)	\tilde{f}_2 (MHz)	$\frac{\tilde{f}_{2,1}-f_{2,1}}{f_{2,1}}$ (PPM)	\tilde{R}_2	$\frac{\tilde{R}_{2,1}-R_{2,1}}{R_{2,1}}$ (PPM)
Single sample rate (Fig. 5)					
$(f_{s,l=1} = f_{s,l=2} = f_{s,l=3} = 5.2 \text{ GSPS})$					
1	0.65	855	1.673×10^{-9}	0.00999967	-12.626
2	3.25	851	-1.4008×10^{-10}	0.01	-0.435
3	5.87	852	-4.1975×10^{-10}	0.00999999	-1.022
Single sample rate (Fig. 5)					
$(f_{s,l=1} = f_{s,l=2} = f_{s,l=3} = 1 \text{ GSPS})$					
1	0.65	855	1.394×10^{-10}	0.00999972	-280.47
2	3.25	851	0	0.00999986	-14.49
3	5.87	852	-1.399×10^{-9}	0.00999958	-41.67
Single sample rate (Fig. 5)					
$(f_{s,l=1} = f_{s,l=2} = f_{s,l=3} = 65 \text{ MSPS})$					
1	0.65	855	0	0.0110381	103813
2	3.25	851	0	0.00997808	-2192.43
3	5.87	852	-0.0925723	0.0100322	3219.53
Dynamic sample rate with $N_M = 24$ (Fig. 12)					
$(f_{s,l=1} = 240 \text{ MHz}, f_{s,l=2} = 48 \text{ MHz}, f_{s,l=3} = 96 \text{ MHz})$					
1	0.65	855	3.137×10^{-8}	0.01	427.17
2	3.25	851	-1.129×10^{-7}	0.01	426.90
3	5.87	852	1.602×10^{-5}	0.01	363.60

Table 4 Comparison of weak signal parameter estimates \tilde{f}_2 and \tilde{R}_2 obtained with dynamic sample rate with estimates obtained with a single sample rate for $N = 2$ simultaneous signals for weak signal parameters $f_{2,j=1} = 3955$ MHz, $f_{2,j=2} = 3951$ MHz, $f_{2,j=3} = 3952$ MHz, and $R_{2,j=1} = R_{2,j=2} = R_{2,j=3} = 0.01$

l	t (μ s)	\tilde{f}_2 (MHz)	$\frac{\tilde{f}_{2,1}-f_{2,1}}{f_{2,1}}$ (PPM)	\tilde{R}_2	$\frac{\tilde{R}_{2,1}-R_{2,1}}{R_{2,1}}$ (PPM)
Single sample rate (Fig. 4)					
$(f_{s,j=1} = f_{s,j=2} = f_{s,j=3} = 5.2$ GSPS)					
1	0.65	3955	-2.41131×10^{-10}	0.00999987	-12.626
2	3.25	3951	-2.74841×10^{-6}	0.01	-0.434484
3	5.87	3952	1.80986×10^{-9}	0.00999999	-1.02269
Single sample rate (Fig. 4)					
$(f_{s,j=1} = f_{s,j=2} = f_{s,j=3} = 1$ GSPS)					
1	0.65	3955	3.61697×10^{-10}	0.0099972	-280.47
2	3.25	3951	3.62063×10^{-10}	0.0099986	-14.4905
3	5.87	3952	7.23943×10^{-10}	0.0099958	-41.6729
Single sample rate (Fig. 4)					
$(f_{s,j=1} = f_{s,j=2} = f_{s,j=3} = 65$ MSPS)					
1	0.65	3955	0	0.00999998	-2.14799
2	3.25	3951	4.82751×10^{-10}	0.01	-0.316919
3	5.87	3952	-2.41314×10^{-10}	0.00999999	-1.24296
Dynamic sample rate with $N_M = 24$ (Fig. 16)					
$(f_{s,j=1} = 240$ MHz $f_{s,j=2} = 48$ MHz $f_{s,j=3} = 96$ MHz)					
1	0.65	3955	0	0.01	-280.47
2	3.25	3951	-4.82751×10^{-10}	0.01	-14.4904
3	5.87	3952	1.20657×10^{-10}	0.01	-41.6727

are much lower than the results achieved with $f_s = 65$ MSPS where the relative error in the weak signal amplitude ranges from approximately -2192 PPM to 3219 PPM.

Table 4 shows a comparison of the relative error in the weak signal frequency estimates using $f_s = 5.2$ GSPS (Fig. 14), 1 GSPS (Fig. 15), and 65 MSPS (Fig. 16). These values for the relative error in the weak signal parameters are lower when dynamic sampling is used in each tier (Fig. 17).

By comparison, use of a dynamic sample rate with $N_M = 24$ in each tier provides weak signal parameter estimates with lower relative error in the weak signal parameter estimates. In conclusion, this paper demonstrates a capability for obtaining accurate estimates of weak signal parameters using dynamic sampling in a multi-tier weak radio frequency signal estimation process. Results show that estimates of the weak signal parameters obtained with dynamic sampling are more accurate compared with estimates obtained with a single sample rate. Future work will take into account the quantization error introduced by an ADC in the sampling process.

Table 5 Comparison of weak signal parameter estimates \tilde{f}_2 and \tilde{R}_2 obtained with dynamic sample rate with estimates obtained with a single sample rate for $N = 2$ simultaneous signals for weak signal parameters $f_{2,j=1} = 5955$ MHz, $f_{2,j=2} = 5951$ MHz, $f_{2,j=3} = 5952$ MHz, and $R_{2,j=1} = R_{2,j=2} = R_{2,j=3} = 0.01$

l	t (μ s)	\tilde{f}_2 (MHz)	$\frac{\tilde{f}_{2,1}-f_{2,1}}{f_{2,1}}$ (PPM)	\tilde{R}_2	$\frac{\tilde{R}_{2,1}-R_{2,1}}{R_{2,1}}$ (PPM)
Single sample rate (Fig. 19)					
$(f_{s,j=1} = f_{s,j=2} = f_{s,j=3} = 5.2$ GSPS)					
1	0.65	5955	-6.40587×10^{-10}	0.00999987	-12.6251
2	3.25	5951	0	0.01	-0.43865
3	5.87	5952	0	0.00999999	-1.02269
Single sample rate (Fig. 20)					
$(f_{s,j=1} = f_{s,j=2} = f_{s,j=3} = 1$ GSPS)					
1	0.65	5955	0	0.0	-280.47
2	3.25	5951	-3.20509×10^{-10}	0.0	-14.4913
3	5.87	5952	1.60228×10^{-10}	0.0	-41.6746
Single sample rate (Fig. 21)					
$(f_{s,j=1} = f_{s,j=2} = f_{s,j=3} = 65$ MSPS)					
1	0.65	5955	0	0.00999998	-2.14798
2	3.25	5951	-6.41018×10^{-10}	0.01	-0.315717
3	5.87	5952	2.08296×10^{-9}	0.00999999	-1.24617
Dynamic sample rate with $N_M = 24$ (Fig. 22)					
$(f_{s,j=1} = 240$ MHz, $f_{s,j=2} = 48$ MHz, $f_{s,j=3} = 96$ MHz)					
1	0.65	5955	2.4022×10^{-9}	0.01	427.162
2	3.25	5951	-1.50639×10^{-8}	0.01	426.913
3	5.87	5952	2.29414×10^{-6}	0.01	363.589

Appendix: Weak 5G simultaneous signals with a strong signal at 5950 MHz and a weak signal at 5955 MHz

We consider another example of two simultaneous 5G signals. The strong signal frequency is $f_1 = 5950$ MHz, and the weak signal is 5955 MHz. Figure 18a–h show the instantaneous frequency $f_{N=2}$ as a function of time (a); estimates of zero crossings $\tilde{t}_{N=2,n}$ as a function of Nyquist multiple N_M (b); difference between estimates of zero crossings and actual zero crossings $\tilde{t}_{N=2,n} - t_{N=2,n}$ as a function of N_M (c); estimates of the weak signal amplitude \tilde{R}_2 as a function of N_M (d); estimates of weak signal frequency \tilde{f}_2 as a function of N_M (e); difference between weak signal amplitude estimates and actual weak signal amplitude $\tilde{R}_2 - R_2$ as a function of N_M (f); difference between weak signal frequency estimates and actual weak signal frequency $\tilde{f}_2 - f_2$ as a function of N_M (g); and relative error in the weak signal amplitude $\frac{\tilde{R}_2 - R_2}{R_2}$ as a function of N_M (h).

We next consider three values of the sample rate of the instantaneous frequency for the two simultaneous 5G signals. Figures 19a–g, 20a–g, and 21a–g show results for the case in which the sample rate $f_s = 5.2$ GSPS, $f_s = 1$ GSPS, and $f_s = 65$ mspS respectively, and the strong signal has $f_1 = 5950$ MHz. The results in the figure show the instantaneous frequency with weak signal frequency $f_2 = 5955$ MHz; $f_2 = 5951$ MHz; $f_2 = 5952$ MHz, respectively, in the three tiers (a); zero crossings in the instantaneous

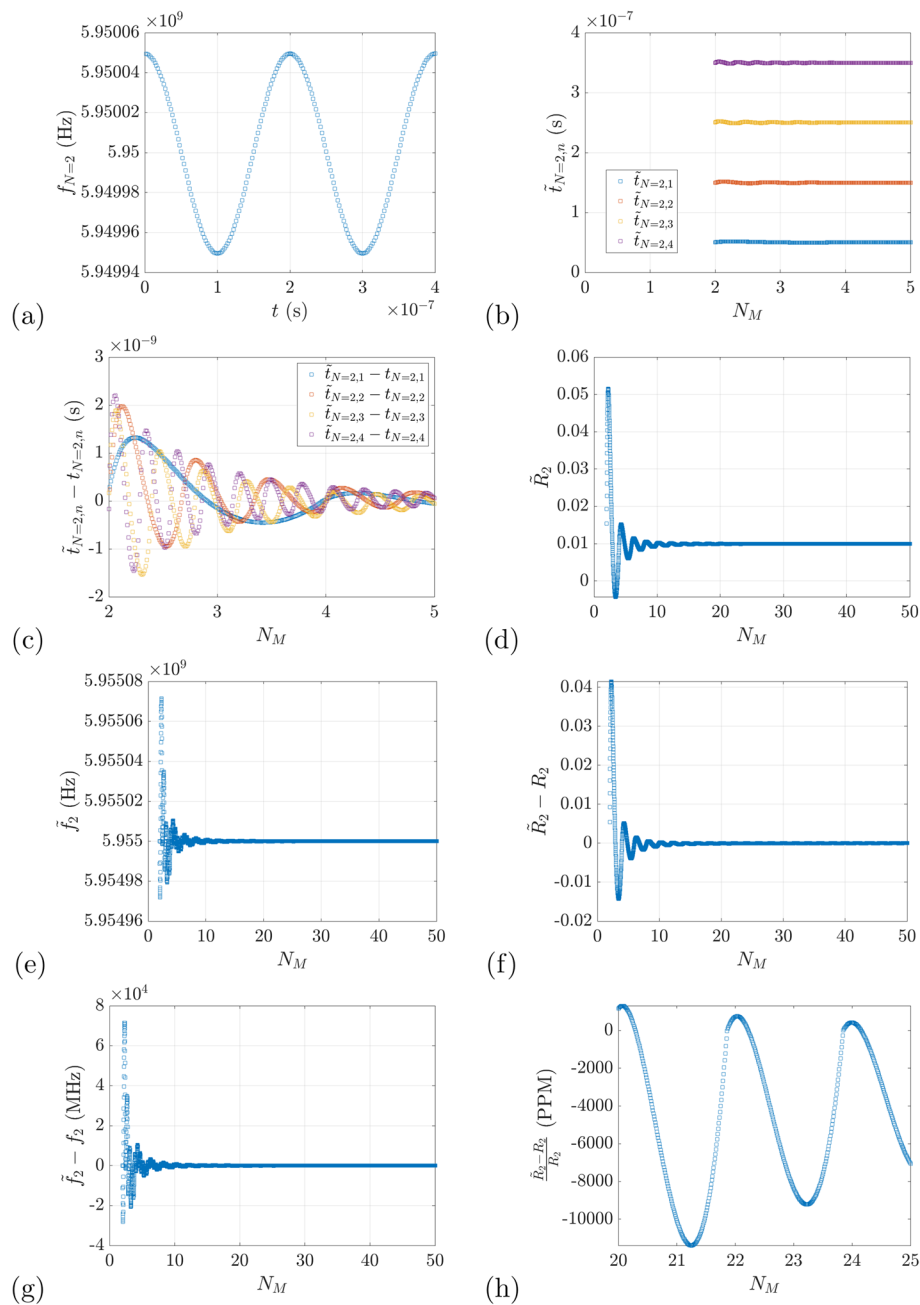


Fig. 18 Strong signal with $f_1 = 5950\text{MHz}$: **a** instantaneous frequency; **b** estimates of zero crossings as a function of Nyquist multiple N_M ; **c** difference between estimates of zero crossings and actual zero crossings as a function of N_M ; **d** estimates of the weak signal amplitude as a function of N_M ; **e** estimates of weak signal frequency as a function of N_M ; **f** difference between weak signal amplitude estimates and actual weak signal amplitude as a function of N_M ; **g** difference between weak signal frequency estimates and actual weak signal frequency as a function of N_M ; **h** relative error in the weak signal amplitude as a function of N_M

frequency as a function of time (b); estimates and actual value of the weak signal amplitude R_2 (c); estimates and actual value of the weak signal frequency f_2 (d); zero crossing error (e); relative error in the weak signal frequency f_2 (f); and relative error in the weak signal amplitude R_2 (g).

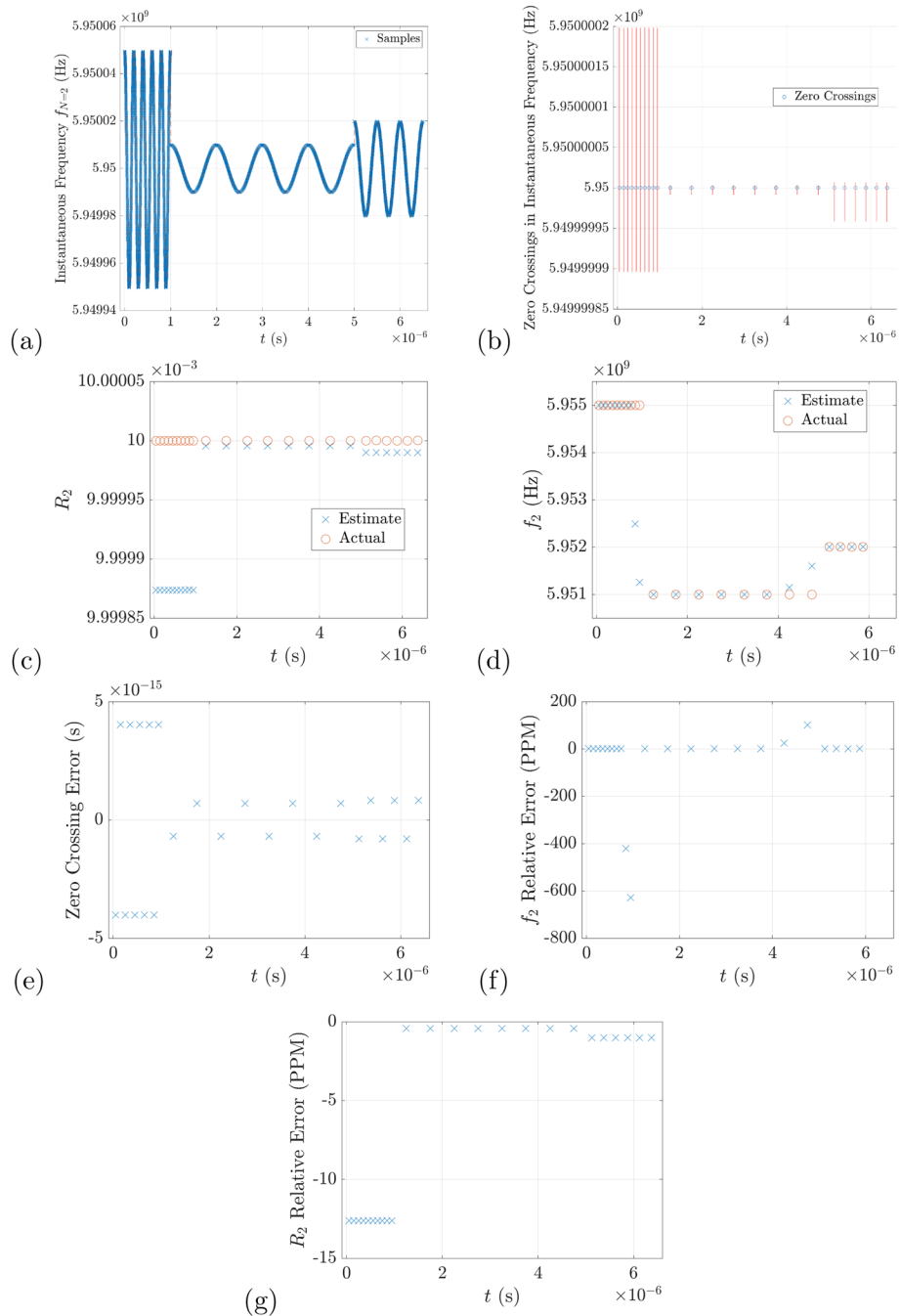


Fig. 19 Sample rate $f_s = 5.2$ GPS and strong signal with $f_1 = 5950$ MHz: **a** instantaneous frequency with weak signal frequency $f_2 = 5955$ MHz; $f_2 = 5951$ MHz; $f_2 = 5952$ MHz, respectively, in the three tiers; **b** zero crossings in the instantaneous frequency as a function of time; **c** estimates and actual value of the weak signal amplitude R_2 ; **d** estimates and actual value of the weak signal frequency f_2 ; **e** zero crossing error; **f** relative error in the weak signal frequency f_2 ; **g** relative error in the weak signal amplitude R_2

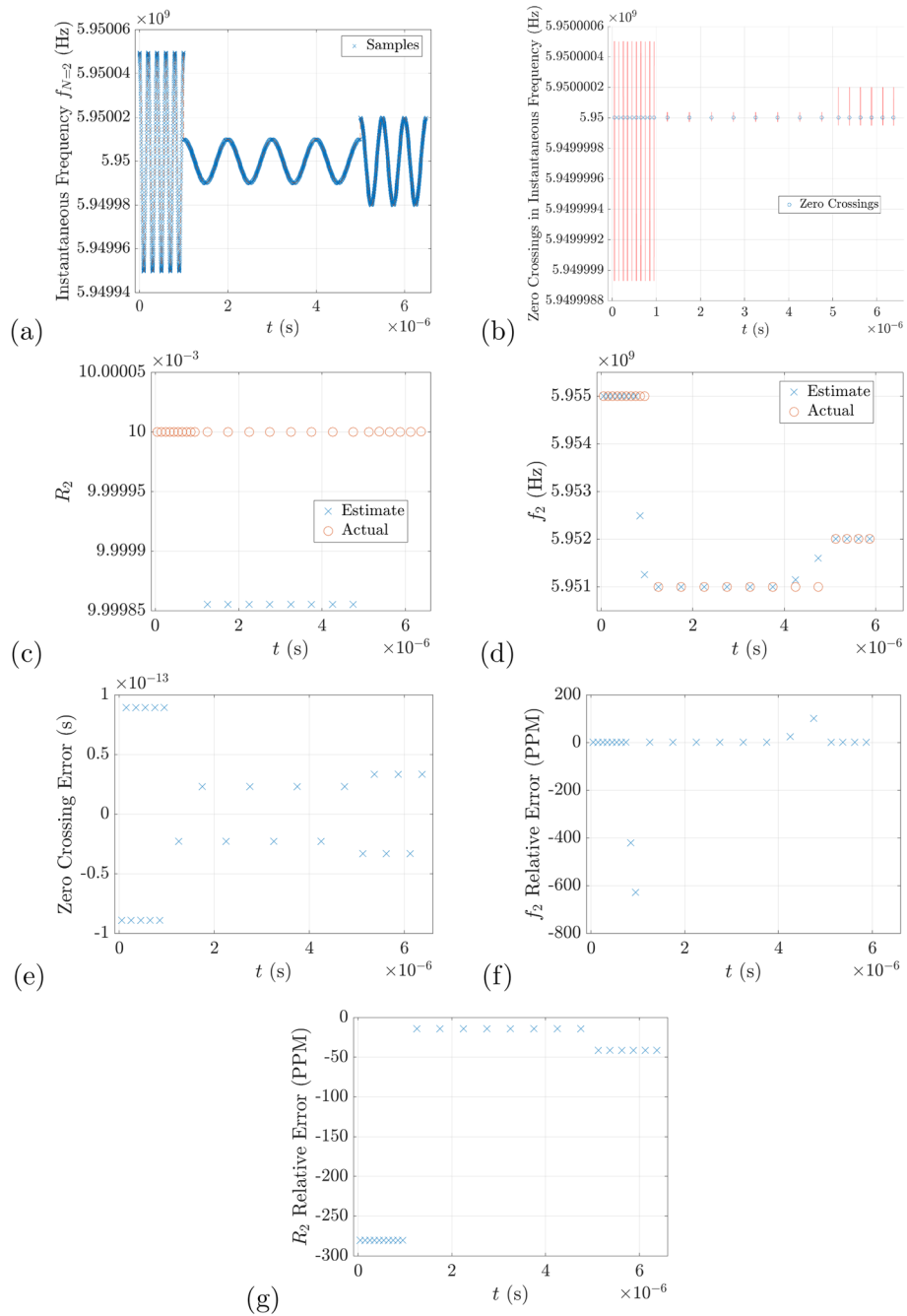


Fig. 20 Sample rate $f_s = 1\text{GSPS}$ and strong signal with $f_1 = 5950\text{MHz}$; **a** instantaneous frequency with weak signal frequency $f_2 = 5955\text{MHz}$; $f_2 = 5951\text{MHz}$; $f_2 = 5952\text{MHz}$, respectively, in the three tiers; **b** zero crossings in the instantaneous frequency as a function of time; **c** estimates and actual value of the weak signal amplitude R_2 ; **d** estimates and actual value of the weak signal frequency f_2 ; **e** zero crossing error; **f** relative error in the weak signal frequency f_2 ; **g** relative error in the weak signal amplitude R_2

We obtain accurate weak signal frequency estimate for the weak 5G signal using dynamic sampling. Figure 22a–h show dynamic sampling at 5950 MHz with three tiers where sampling rate f_s changes based on data collected in real time. The figure shows the instantaneous frequency as a function of time (a); instantaneous frequency with zero

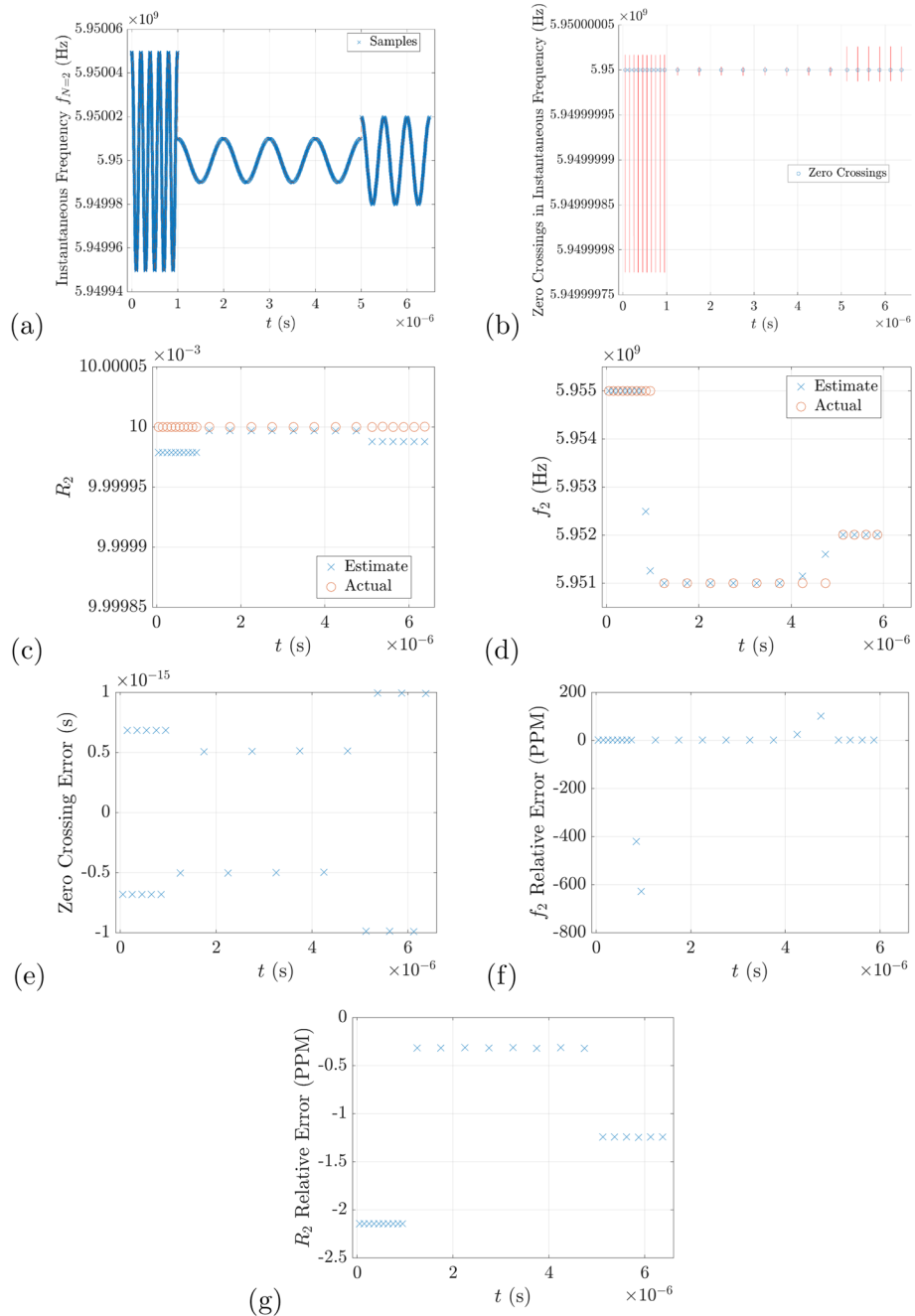


Fig. 21 Sample rate $f_s = 65$ msp/s and strong signal with $f_1 = 5950$ MHz: **a** instantaneous frequency with weak signal frequency $f_2 = 5955$ MHz; $f_2 = 5951$ MHz; $f_2 = 5952$ MHz, respectively, in the three tiers; **b** zero crossings in the instantaneous frequency as a function of time; **c** estimates and actual value of the weak signal amplitude R_2 ; **d** estimates and actual value of the weak signal frequency f_2 ; **e** zero crossing error; **f** relative error in the weak signal frequency f_2 ; **g** relative error in the weak signal amplitude R_2

crossings (b); estimates and actual weak signal amplitude (c); estimates and actual weak signal frequency (d); zero crossing error (e); relative error in the weak signal frequency estimate (f); relative error in the weak signal amplitude estimate (g); and sample rate in each tier determined based on data collected in real time (h).

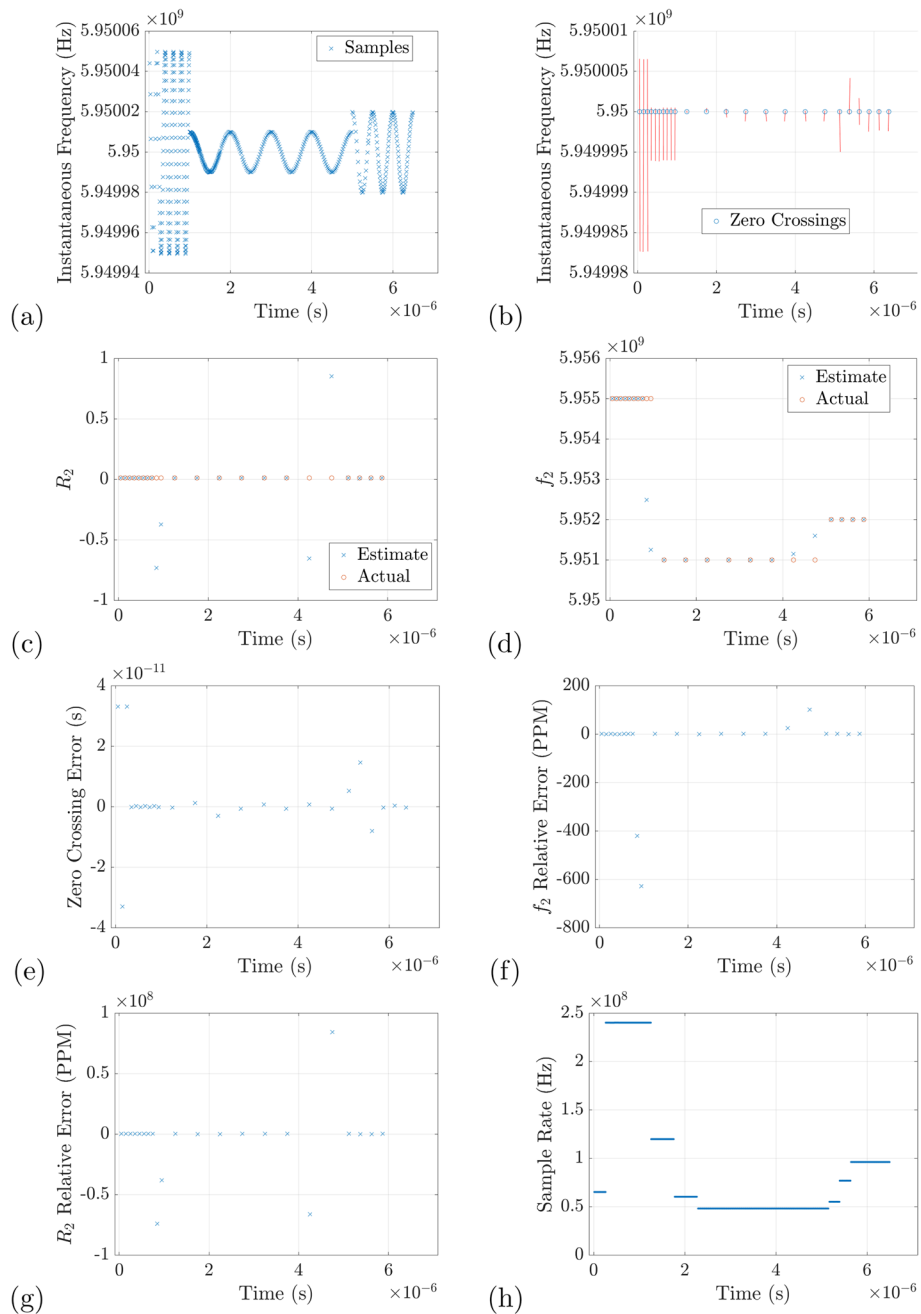


Fig. 22 Dynamic sampling at 5950 MHz with three tiers where sampling rate f_s changes based on data collected in real time: **a** instantaneous frequency as a function of time; **b** instantaneous frequency with zero crossings; **c** estimates and actual weak signal amplitude; **d** estimates and actual weak signal frequency; **e** zero crossing error; **f** Relative error in the weak signal frequency estimate; **g** Relative error in the weak signal amplitude estimate; **h** sample rate in each tier determined based on data collected in real time

Acknowledgements

The authors thank the reviewers for feedback on the manuscript that has greatly improved the paper. The authors thank Muataz Boker and Michael Ruohoniemi for feedback on a paper draft and the Bradley Department of Electrical and Computer Engineering at Virginia Tech for support of this research.

Author contributions

The authors equally contributed to the paper. B.S. wrote the first draft of the paper, with the application, code, and figures. M.L. wrote the theory and revised the drafts of the paper and revised the figures.

Availability of data and materials

Please contact authors for data requests.

Declarations**Competing interest**

The authors declare that they have no competing interests.

Received: 17 July 2023 Accepted: 7 December 2023

Published online: 06 January 2024

References

1. B. Wook Jung, R.S. Adve, J. Chun, M.C. Wicks, Detection performance using frequency diversity with distributed sensors. *IEEE Trans. Aerosp. Electron. Syst. (TAES)* **47**(3), 1800–1813 (2011)
2. F. Digne, A. Baussard, A. Khenchaf, Classification of radar pulses in a naval warfare context using bezier curve modeling of the instantaneous frequency law. *IEEE Trans. Aerosp. Electron. Syst. (TAES)* **53**(3), 1469–1480 (2017)
3. D. Adamy, *EW 101: A First Course in Electronic Warfare* (Artech House, Norwood, MA, 2001)
4. R. Wiley, *ELINT: The Interception and Analysis of Radar Signals* (Artech House, Norwood, MA, 2006)
5. P.W. East, *Fifty Years of Instantaneous Frequency Measurement* (IET Radar, Sonar Navig, 2012)
6. S. J. Robinson, N. E. Goddard, Broadband Hybrid Junction. British Patent, 818018 (1957)
7. S. J. Robinson, Broadband Hybrid Junctions. *IRE Trans. MTT8*, pp. 671–672 (1960)
8. S. J. Robinson, Broadband Microwave Discriminator. British Patent, 953430 (1958)
9. S. J. Robinson, Comment on Broadband Microwave Discriminator. *IEEE Trans. MTT12*, (1964)
10. J. C. Walling, The Mullard/Philips Research Laboratories, Redhill. A Short History 1946–2002. Philips Electronics UK Ltd (2005)
11. K. George, C.-I.H. Chen, Multiple signal detection digital wideband receiver using hardware accelerators. *IEEE Trans. Aerosp. Electron. Syst.* **49**(2), 706–715 (2013)
12. P.-J. Chung, J. F. Bohme, C. F. Mecklenbrauker, A. O. Hero, Multiple signal detection using the Benjamini-Hochberg procedure, in *Proceedings of the 1st IEEE International Workshop on Computational Advances in Multi-Sensor Adaptive Processing*, Puerto Vallarta, Mexico, 209–212 (2005)
13. G. Lopez-Risueno, J. Grajal, Multiple signal detection and estimation using atomic decomposition and EM. *IEEE Trans. Aerosp. Electron. Syst.* **42**(1), 84–102 (2006)
14. G. Lopez-Risueno, J. Grajal, A. Sanz-Osorio, Digital channelized receiver based on time-frequency analysis for signal interception. *IEEE Trans. Aerosp. Electron. Syst.* **41**(3), 879–898 (2005)
15. K. George, C.-I.H. Chen, Multiple signal detection and measurement using a configurable wideband digital receiver, in *Proceedings of IEEE International Instrumentation and Measurement Technology Conference*, Warsaw, Poland, May, 1–5 (2007)
16. P. Raviteja, K.T. Phan, Y. Hong, E. Viterbo, Orthogonal time frequency space (OTFS) Modulation Based Radar System, in *2019 IEEE Radar Conference*, Boston, MA, 22–26 (2019). <https://ieeexplore.ieee.org/document/8835764>
17. W. Dong, Y. Wang, G.C. Sun, M. Xing, Passive localization for frequency hopping signal emitter based on synthetic aperture principle. *IEEE J. Min. Air Space Syst.* **4**(1), 33–40 (2022)
18. S. Alphonse, G.A. Williamson, On estimating nonlinear frequency modulated radar signals in low SNR environments. *IEEE Trans. Aerospace Electron. Syst.* **57**(3), 1793–1802 (2021)
19. G.-C. Liang, C.-F. Shih, R.S. Withers, B.F. Cole, M.E. Johansson, Space-qualified superconductive digital instantaneous frequency measurement subsystem. *IEEE Trans. Microw. Theory Tech.* **44**(7), 1289–1299 (1996)
20. W. Khalil, B. Bakkaloglu, S. Kiaei, A self-calibrated on-chip phase-noise measurement circuit With -75 dBc single-tone sensitivity at 100 kHz offset. *IEEE J. Solid-State Circuits* **42**(12), 2758–2765 (2007)
21. D. Lam, B.W. Buckley, C.K. Lonappan, A.M. Madni, B. Jalali, Ultra-wideband instantaneous frequency estimation. *IEEE Instrum. Meas. Mag.* **18**(2), 26–30 (2015)
22. A. Goavec, R. Vauche, J. Gaubert, F. Hameau, M. Zarudniev et al., Instantaneous frequency measurement for IR-UWB signal in CMOS 130 nm, in *2016 IEEE International Conference on Electronics, Circuits and Systems (ICECS)*, Monte Carlo, Monaco, 157–160 (2016)
23. X. Wang, S. Pan, Broadband microwave measurement based on photonics technologies, in *2016 15th International Conference on Optical Communications and Networks (ICOON)* (2016)
24. S. Pan, J. Yao, Photonics-based broadband microwave measurement. *J. Lightwave Technol.* **35**(16), 3498–3513 (2017)
25. F. Zhou, H. Chen, X. Wang, L. Zhou, J. Dong, X. Zhang, Photonic multiple microwave frequency measurement based on frequency-to-time mapping. *IEEE Photon. J.* **10**, 1–7 (2018)
26. J. Shi, F. Zhang, D. Ben, S. Pan, Photonics-based broadband microwave instantaneous frequency measurement by frequency-to-phase-slope mapping. *IEEE Trans. Microwave Theory Tech.* **67**(2), 544–552 (2019)
27. Z. Tang, P. Zhou, J. Zhu, N. Li, Photonics-based microwave frequency measurement with broadband signal generation and processing, in *2022 Asia Communications and Photonics Conf. (ACP) and International Conference on Information Photonics and Optical Communications (IPOC)*, L785–L788 (2022)
28. P. Zhou, Z. Tang, J. Zhu, N. Li, Instantaneous frequency measurement using photonics-assisted broadband signal generation and processing. *IEEE Microwave and Wireless Tech. Lett.* **33**(5) (2023)

29. Z. Bai, S. Li, X. Xue, X. Zheng, Ultra-wideband instantaneous frequency measurement based on differential photonic time-stretch. *Opt. Comm.* **541**(15), 129516 (2023)
30. L. Baldini, D. Manstretta, T. Erseghe, N. Laurenti, A. Liscidini, R. Castello, Reconfigurable multi-band OFDM UWB receivers: circuits and system considerations, in *Circuits and Systems for Future Generations of Wireless Communications, Tasic et al. Series on Integrated Circuits and Systems, Chapter 3*, Springer Science+Business Media B.V. (2009), https://link.springer.com/chapter/10.1007/978-1-4020-9917-5_3
31. M.R. LeRoy, S. Raman, M. Chu, J.-W. Kim, J.-R. Guo, K. Zhou, C. You, R. Clarke, B. Goda, J.F. McDonald, High-speed reconfigurable circuits for multirate systems in SiGe HBT technology. *Proc. IEEE* **103**(7), 1181–1196 (2015)
32. M.Y. Lanzerotti, A. Queen, C. Cerny, Quantization error for weak RF simultaneous signal estimation. *EURASIP J. Adv. Signal Process.* (2023). <https://doi.org/10.1186/s13634-023-01046-7>
33. M.Y. Lanzerotti, C. Cerny, R. K. Martin, Phase calculation approaches for a multi-tier weak radio signal detection process with N simultaneous signals. in *Proceedings of the NAECON, Dayton, OH*, pp. 277–284 (2014)
34. M.Y. Lanzerotti, C. Cerny, A theoretical phase calculation approach for N simultaneous signals. *IEEE Trans. Aerospace Electron. Syst.* **51**(2), 878–883 (2015)
35. M.Y. Lanzerotti, C. Cerny, R.K. Martin, Ultraweak simultaneous signal detection with theoretical phase calculation approaches. *IEEE Trans. Aerospace Electron. Syst.* **51**(2), 884–893 (2015)
36. M.Y. Lanzerotti, C. Cerny, R. K. Martin, Phase measurement approaches for a multi-tier weak radio signal detection process with N simultaneous signals having continuous phase. in *Proceedings of the NAECON, Dayton, OH*, pp. 1–7 (2015)
37. M.Y. Lanzerotti, C. Cerny, R.K. Martin, Error in parameter estimation in a multi-tier weak radio signal detection process with N simultaneous signals having continuous phase. in *Proceedings of the NAECON, Dayton, OH*, pp. 1–9 (2016)
38. M.Y. Lanzerotti, C. Cerny, R. K. Martin, Quantifying error estimates as functions of signal-to-noise ratio in a multi-tier weak radio signal detection process with N simultaneous signals. in *Proc. NAECON, Dayton, OH*, pp. 1–13 (2018)
39. M.Y. Lanzerotti, C. L. Cerny, M. Current, R. K. Martin, Noisy simultaneous signal parameter estimation with generalized phase calculation approaches. in *Proceedings of the AIAA SciTech 2021 Forum*, 19–21 (2021). Virtual Event
40. J. Tsui, *Digital Techniques for Wideband Receivers*, 2nd edn. (Scitech Pub, Edison, NJ, 2004)
41. D. Thompson, Troubleshooting weak 5G signal: expert recommendations, March 13 (2023). <https://www.sciencetimes.com/articles/42785/20230313/troubleshooting-weak-5g-signal-expert-recommendations.htm#:~:text=Understanding%20the%20Causes%20of%20Weak,vital%20to%20finding%20a%20solution>
42. F.L. Luo, C. Zhang (Eds.) *Signal processing for 5G: algorithms and implementations*, Wiley-IEEE Press (2016). <https://ieeexplore.ieee.org/book/7572254>
43. M. Rowe, DSP core processes 5G baseband data, May 18, (2020). <https://www.5gtechnologyworld.com/dsp-core-processes-5g-baseband-data/>

Publisher's Note

Springer Nature remains neutral with regard to jurisdictional claims in published maps and institutional affiliations.

Submit your manuscript to a SpringerOpen[®] journal and benefit from:

- Convenient online submission
- Rigorous peer review
- Open access: articles freely available online
- High visibility within the field
- Retaining the copyright to your article

Submit your next manuscript at ► [springeropen.com](https://www.springeropen.com)
